Perspectives on ultra-high vacuum transmission electron microscopy of dynamic crystal growth phenomena

Perspectives on ultra-high vacuum transmission electron microscopy of dynamic crystal growth phenomena

Kate Reidy[1], Joachim Dahl Thomsen[1], Frances M. Ross[1 *]

1. Department of Materials Science and Engineering, Massachusetts Institute of Technology, Cambridge, MA, United States

*Correspondence: fmross@mit.edu

Abstract: Crystal nucleation and growth is a fundamental pillar of materials design. To advance our understanding of the underlying mechanisms, *in situ* visual observation plays an important role by providing dynamic information unavailable through conventional post-growth analysis. Such information includes nucleation and growth rates, diffusion phenomena, phase transformation kinetics, strain relaxation mechanisms, and defect formation. Here, we review the contributions of ultra-high vacuum transmission electron microscopy (UHV-TEM) to our understanding of dynamic crystal growth phenomena. We describe the vacuum, sample handling, and deposition capabilities essential for quantitative studies of reactive metals and semiconductors, and discuss how these capabilities are achieved while preserving the imaging performance of the microscope. We then show examples of growth processes explored using UHV-TEM, where the high spatial and temporal resolution provides unique insights into nanocrystal nucleation, thin film microstructure evolution, and oxidation in controlled environments. We assess these past accomplishments in the context of recent advances in transmission electron microscopy, discussing how aberration correction, modified sample environments, fast and sensitive detectors, and data science are unlocking powerful opportunities for atomic and temporal resolution measurements using UHV-TEM. We conclude by discussing the challenges and future perspectives for scientific advances using this technique.

1. Introduction

Tailoring crystal nucleation and growth to control the resulting structure is central to materials design.[1–3] Understanding key phenomena occurring during materials growth helps to achieve desirable mechanical, chemical, electrical, magnetic, optical, and biomedical properties. *In situ* visual observation plays an important role in advancing our understanding of crystal growth phenomena by providing dynamic information unattainable through conventional *ex situ* or post-growth analysis. This information includes nucleation and growth kinetics, diffusion and coalescence, mechanisms of epitaxy, strain relaxation, and reaction rates during phenomena such as phase transformations, catalysis, oxidation, and etching.[4–9] Among current state-of-the-art *in situ* techniques for studying crystal growth - such as *in situ* x-ray, neutron, and optical spectroscopy studies[10] - *in situ* transmission electron microscopy (TEM) and scanning transmission electron microscopy (STEM) are becoming increasingly powerful. Recent advances in instrumentation and data analysis techniques, including aberration correction, stable *in situ* holders, microfabricated chips, fast and sensitive detectors, and larger pole-piece gaps, enable ever more precise control of sample environment. This is unlocking opportunities for atomic and temporal resolution measurements using *in situ* (S)TEM.[11–17]

In situ ultra-high vacuum (UHV)-TEM represents a subset of *in situ* (S)TEM techniques. A UHV-TEM consists of an electron microscope[*1] modified to achieve UHV (~ 10^{-10} Torr) at the sample region. Capabilities such as sample heating, gas injection, physical vapor deposition, molecular beam epitaxy, and chemical vapor deposition are often integrated within the microscope system.[4] This allows material growth to be carried out during imaging to create real-time 'movies' of crystal growth phenomena with up to atomic resolution. The UHV

[*1] We use the term 'UHV-TEM' to include both UHV-TEM and UHV-STEM. Where *in situ* UHV-STEM studies are described, the distinction is noted where relevant. We also utilize the acronym 'TEM' to refer to both the instrument (i.e. transmission electron microscope) and technique (i.e. transmission electron microscopy) throughout the manuscript, as is common in literature.

environment minimizes the levels of background gases and contamination, and the ability to form atomically clean surfaces provides an ideal playground to quantify the kinetics and thermodynamics of crystal growth. This is particularly important in the study of nanocrystal and thin film growth, where adsorbed species on the starting surface can greatly affect kinetic mechanisms.[4–9] It also helps reduce unwanted side reactions, enabling more precise measurements of processes of interest, such as oxidation, catalysis, and other scientifically important and technologically relevant processes.[18]

In this review we describe the contributions that *in situ* UHV-TEM has made to our understanding of nucleation and growth phenomena. Although UHV-TEM has contributed to other fields, notably in measuring the structure of surfaces,[19–22] we limit the scope of this review to studies of nucleation and growth. We describe the vacuum, sample handling, and deposition capabilities necessary for quantitative studies of reactive materials in controlled UHV environments (**Section 2**), and how these capabilities are achieved while preserving the imaging performance of the microscope (**Section 3**). We then showcase examples where *in-situ* experiments using UHV-TEM have provided unique insights into nanocrystal nucleation and growth (**Section 4.1**), thin film microstructure evolution (**Section 4.2**), and gas-phase reactive growth processes (**Section 4.3**). We conclude that advances made through UHV-TEM over its history underpin our understanding of key materials processes. Finally, we discuss challenges in the field of *in situ* UHV-TEM and consider how the microscopy community's prior experience in UHV microscopy will combine with present day instrumentation to unlock future transformative materials design opportunities using *in situ* UHV-TEM (**Section 5**).

2. The motivation for *in situ* UHV-TEM for crystal growth studies

2.1 Why ultra-high vacuum?

To extract quantitative information on the thermodynamics and kinetics of crystal growth, the structure and surface of the sample should be well-controlled initially and remain so throughout the experiment. A UHV environment helps minimize heterogeneous sites for nucleation, uncontrolled chemistry, and competing reactions between the materials of interest and environmental components such as water vapor or oxygen. Consequently, UHV conditions are often utilized in surface science experiments involving techniques such as scanning tunnelling microscopy (STM), x-ray photoelectron spectroscopy (XPS), angle-resolved photoelectron spectroscopy (ARPES), and secondary ion mass spectroscopy (SIMS).[23,24] Although some surface science techniques utilize near-ambient pressures,[25] a UHV sample environment ensures surface cleanliness, prevents side reactions, and clarifies the effects of process variables such as temperature or flux.

Reactions that benefit from UHV environment studies include nanocrystal nucleation and growth, thin film epitaxy, atomic layer deposition, surface reactions, chemisorption, molecular beam epitaxy, oxidation, certain dislocation and grain boundary dynamics, surface reconstructions, and gas/catalyst/support interactions.[5,18,21,26–32] Similarly, the synthesis and processing of many technologically important metals (e.g. Zr, Ti, Ta, Nb, Mo, Fe and Cu) and semiconductors (e.g. Si, Ge, GaAs) are highly sensitive to trace impurities and require the ultra-clean environment associated with UHV.[33]

The practicalities of achieving UHV conditions can best be illustrated by a back of the envelope calculation using the Langmuir equation, which gives the time, τ, for a monolayer of atoms to adsorb on the surface of a sample:

$$\tau = \frac{\Sigma_s}{P}(2\pi m k_B T)^{\frac{1}{2}}$$

Here Σ_s is the areal density of atoms, P is the pressure, m is the mass of the atom, k_B is Boltzmann's constant, and T is the absolute temperature. A typical surface exhibits an areal density of the order of 10^{15} atoms/cm^2. Therefore, at atmospheric pressure (P = 760 Torr), the monolayer formation time, τ, is ~10^{-9} seconds. This means that any surface exposed to atmosphere is covered with a monolayer of atoms within a nanosecond. At the vacuum available in conventional TEMs (P = 10^{-6} – 10^{-7} Torr), τ = 3 - 30 seconds, still unsuitable for *in situ* experiments on clean surfaces. UHV conditions (P = 10^{-10} Torr) bring the monolayer formation time to ~10 hours. This allows time for an *in situ* experiment where processes that require ultra-clean surfaces and low levels of adsorbed impurities can be studied.

2.2 Why transmission electron microscopy?

UHV conditions are challenging to engineer in TEM instruments due to the restricted geometry around the sample, the variety of materials present in the holder, goniometer, and polepiece that are not UHV-compatible, and the need to avoid vibrations from pumps. Despite these challenges, many researchers are motivated to design and build such instruments due to the power of UHV-TEM to solve materials problems. In particular, the combination of spatial and temporal resolution offered by TEM is difficult to obtain from any other single technique. Scanning probe microscopes, for example, offer exceptional spatial resolution but (except under special circumstances) require minutes or longer to complete each scan. Spectroscopic methods such as XPS and ARPES provide rapid data acquisition but compromise spatial resolution and can be limited to the sample surface. TEM has a fast acquisition speed and can probe beneath material surfaces, providing information on buried interfaces, defects, compositional variations, and strain fields (within the constraints of the sample thickness). Moreover, the variety of imaging modes available in TEM enables a flexible approach to problem solving through combinations of techniques, such as bright and dark field imaging, high-resolution phase contrast, diffraction, electron energy loss spectroscopy (EELS), and focused probe imaging modes such as ptychography and 4D STEM. As discussed further in **Section 5**, correlative studies that leverage the spatial and temporal benefits of TEM *alongside* the advantages of scanning probe microscopy, surface science, or spectroscopic techniques can enable experimental realizations surpassing those possible by any individual technique.[4,34–36]

2.3 Why *in situ*?

In situ UHV-TEM enables temporally resolved imaging, facilitating direct observation and quantification of dynamic processes, visualization of the response of the material to specific stimuli, and a rapid survey of relevant parameter spaces. Various other *in situ* TEM customizations have been developed to explore dynamic systems and processes at the nanoscale, including liquid cell TEM,[13] ultrafast TEM,[37] and environmental TEM (ETEM).[38] The sample may be heated, cooled, or electrically biased using *in situ* sample holders and microelectromechanical (MEMS) chips,[39] while multi-modal capabilities enable structure, composition, and property measurements.[40] Although *in situ* TEM and *in situ* holders have existed for decades,[41] current advances in high-speed data acquisition, detector technology, data storage, and low-drift stages have made time-resolved imaging one of the most active frontiers of TEM.[11]

Combining the above considerations, *in situ* UHV-TEM can be regarded as a technique that possesses three key features: temporal resolution, spatial resolution, and controlled environment. This third feature entails not only achieving UHV around the sample but also incorporating heating, deposition, and other tools necessary for *in situ* sample modification. Attaining any two of these features already yields rich opportunities (**Figure 1, side panels**). However, all three together produce a uniquely powerful tool to study thermodynamic and kinetic processes at the intersection of materials science, physics, chemistry, and nanotechnology (**Figure 1**).

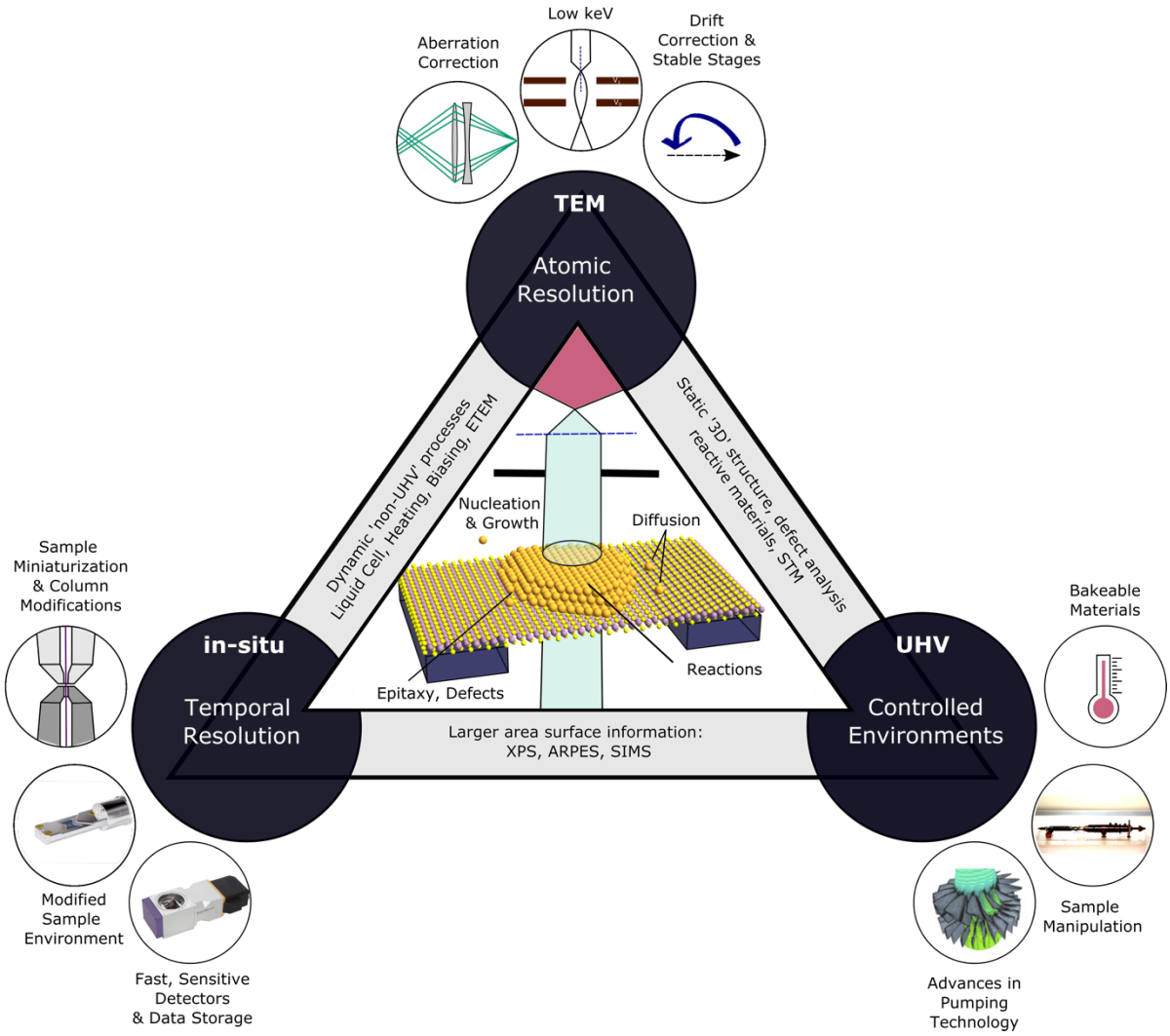

Figure 1: Schematic illustrating the benefits of combining atomic resolution, temporal resolution, and controlled environment for materials growth studies. Combining pairs of these factors is shown along the triangle edges: ***in situ* TEM** can study dynamic 'non-UHV' processes, such as those in liquid phase, but cannot study kinetics in ultra-clean environments; other ***in situ* UHV** techniques can access growth kinetics at the nanoscale, but may be limited to surfaces or lack spatial resolution; static **UHV-TEM** provides snapshot measurements of surface and subsurface structures for materials that react readily with the environment. ***In situ* UHV-TEM** (triangle center) enables study of dynamic processes in controlled environments with atomic and temporal resolution. Small circles show areas that have advanced particularly over the past decade to bring *in situ* UHV-TEM closer to widespread distribution. Image credits for insets: Protochips Inc. for 'Modified Sample Environment'[42]; Direct Electron for 'Fast, Sensitive Detectors'[43]; Denis Paiste, MIT, for image in 'Sample Manipulation'.

3. Historical development of *in situ* UHV-TEM instrumentation and current state-of-the art

Starting from a TEM design that provides the necessary spatial and temporal resolution, several objectives must be achieved when constructing an *in situ* UHV-TEM instrument to study dynamic materials processes. First, the UHV sample environment must be achieved. Second, *in situ* capabilities within the TEM column, such as sample heating, biasing, physical deposition, or gas dosing, need to be designed. Finally, for maximum flexibility and impact, it is helpful to integrate the microscope with other capabilities, such as sample preparation, calibration, complementary analytical techniques, and even a garage to hold multiple samples. These capabilities are often housed in side chambers attached to the microscope. Samples can be prepared and transferred under vacuum, enabling sample modification within the UHV environment even if not within the column.

These functions exist to varying extents in the handful of UHV-TEMs that have been built and operated in the past and present day. The functionality of each UHV-TEM is the result of individual choices made by the users and microscope manufacturers, based on specific research needs. In the following paragraphs we discuss instrument design to achieve these functions. Relatively few UHV-TEMs have been constructed, but these instruments have been profoundly productive in fundamental and applied materials science, as we describe in **Section 4**.

3.1 Obtaining a UHV sample environment

Spatial resolution is often seen as the sole progress indicator of electron microscopy. However, over the past 70 years, a dedicated subset of microscopy researchers and companies have focused on advancing the vacuum environment, even compromising on spatial resolution to achieve their objective. Many early *in situ* experiments paved the way for combining both UHV and *in situ* environments.[44–48] From the inception of electron microscopy, the need to maintain some level of vacuum within the column to avoid electron scattering was clear.[49] The importance of UHV conditions was further emphasized by Pashley, Bassett, Stowell, and collaborators in a series of *in situ* TEM studies from the 1950s and 60s, in which gold (Au) was grown on single crystalline surfaces (MoS_2, graphite, mica) in conventional 10^{-6} Torr TEM vacuum.[50,51] A quote from their seminal paper states: '*In view of the limitations of our experimental arrangement, a study of the kinetics of nucleation is not readily possible. It is important to consider how the growth process is influenced by the presence of the residual gases and vapors, and to what extent the process would be modified in a clean ultra-high vacuum system. Unfortunately it is not possible to repeat this type of experiment inside an electron microscope, without considerable re-design and re-building of the microscope.*'[46] This challenge catalyzed the *in situ* UHV-TEM development that continues today.

The historical evolution, both conceptual and practical, of *in situ* UHV-TEM is well-described in a 2004 review article by Poppa,[4] as well as in books featuring instrumental developments from the manufacturers VG and JEOL.[52,53] For this reason, we will not explore the historical context in depth, but focus on the main milestones and current state-of-the-art. **Figure 2** provides a historical timeline of key advances in *in situ* UHV-TEM. Although other UHV-TEMs exist, in order to maintain the scope of this review **Figure 2** aims to focus exclusively on UHV-TEM equipment that *also* allowed for dynamic crystal growth inside the column or in side chambers by incorporating deposition capabilities.

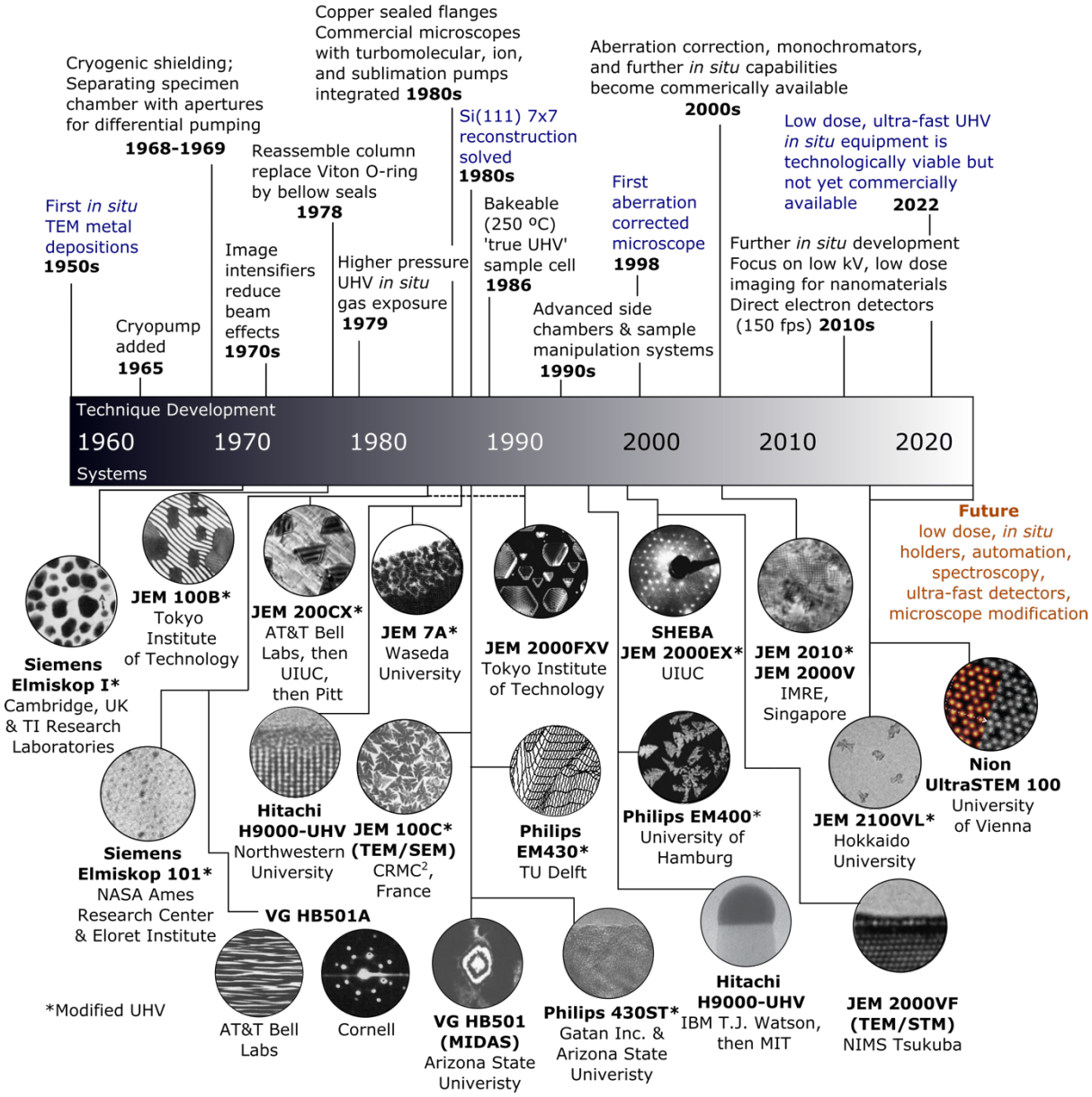

Figure 2: Timeline of some of the major engineering developments that enabled *in situ* UHV-TEM (black, top); broader implications and historic milestones (blue, top), and UHV-TEM equipment with capabilities for *in situ* deposition (bottom). (Top) All historical developments in black are from ref [4]. References for blue milestones: First *in situ* metal depositions[44–47], Si (111) 7x7 reconstruction solved[22], first aberration corrected microscope[17] (**Bottom**) Instruments are 'dated' according to the first peer-reviewed journal describing their construction or use for *in situ* deposition, as known to the authors at the time of publication. Occasionally conference proceedings preceded journal publication, although many are not available online. Therefore, dashed lines account for uncertainties in the instrumentation timeline and this list represents the authors' best attempt at summarizing relevant *in situ* UHV-TEM instrumentation based on sources available: Siemens Elmiskop 1[54], JEM 100B[55,56], Siemens Elmiskop 101[57,58], VG HB501A[32,59], JEM 200 CX[60,61], Hitachi H9000-UHV (Northwestern)[21,62] - with later addition of SPEAR[35], JEM 7A[63], JEM 100C[64], VG HB501 (and MIDAS)[36,65,66], Philips 430ST[67,68], Philips EM430[69], JEM 2000FXV[70,71], Hitachi H9000-UHV

(IBM)[72], Philips EM400[73], SHEBA JEM 2000EX[29,74], JEM 2000VF[75], JEM 2010 & 2000V[76], JEM 2100VL[77], Nion UltraSTEM 100[78,79]. Asterisk indicates that the instrument was not commercially fabricated with UHV capabilities but was later modified for UHV environment. An example image is shown for each, to be discussed further in **Section 4**. References for images from left to right: Siemens Elmiskop 1[54], JEM 100B[55], Siemens Elmiskop 101[57], VG HB501A[32,59], JEM 200 CX[30], Hitachi H9000-UHV (Northwestern)[21], JEM 7A[63], JEM 100C[64], VG HB501 (MIDAS)[65], Philips 430ST[80],Philips EM430[81], JEM 2000FXV[4], Hitachi H9000-UHV (IBM)[82], Philips EM400[31], SHEBA JEM 2000EX[74], JEM 2000VF[28], JEM 2010[76], JEM 2100VL[83], Nion UltraSTEM 100[79].

Initial trials at improving the vacuum condition consisted of surrounding the sample with a cryogenic shield to condense vapor from the column, and improving the pumping speed.[4] Takayanagi *et. al* performed one of the first major modifications to a commercial microscope, a JEM 100B, installing cryoshields, a liquid-nitrogen-trapped oil diffusion pump in the main column, and re-assembling the microscope while cleaning each component (with o-rings of particular importance). This reduced residual vapor around the substrate to 10^{-8} – 10^{-10} Torr without loss of resolution.[55] However, relying on a cryogenic shield for pumping is a drawback for *in situ* studies since it restricts geometric access to the sample for deposition, ion bombardment, and other *in situ* capabilities.[4]

Therefore, other techniques emerged that involved separating the specimen chamber from the column by small apertures or thin film windows. This enabled differential pumping of the sample area, bolstered by advances in pumping technology such as high-speed liquid He cryopumps, vibrationless ion pumps, and Ti sublimation pumps. Moreover, improved materials selection and advances in fabrication and design meant that 'bakeable' systems were developed, which allowed heating of the chamber walls to remove residual vapor by outgassing.[53] The mid 1980s heralded the first such commercially available microscopes that maintained resolution while integrating cleaner pump systems, liner materials for the column that reduced outgassing, and compatibility with mild bake temperatures. VG instruments in particular were UHV and designed for bakeability, including UHV airlock facilities for handling, preparing, and transferring specimens.[53] Custom modifications were carried out in individual labs to bring conventional microscopes to UHV conditions or to add *in situ* deposition capabilities (**Figure 2**). In some cases, UHV systems were fitted with analytical equipment such as Auger electron spectroscopy (AES), and separate specimen chambers were incorporated inside the TEM column, allowing *in situ* capabilities while maintaining UHV environment.[32,36,53,57] However, resolution (in a non-aberration-corrected TEM) is inversely related to pole-piece gap, so increasing this gap to integrate a customized specimen chamber resulted in loss of resolution. Detectors capable of video-rate high-resolution imaging were concurrently developed, simplifying the process of recording high quality data during materials growth and reactions.

Current state-of-the-art in high-resolution *in situ* UHV-TEM lies in rigorous pumping, strategic placement of differential pumping apertures, and selection of microscope materials to minimize outgassing while ensuring all chamber components are bakeable to 120-200 ºC. Some of the first commercially available microscopes designed for *in situ* deposition that adhered to these conditions were the Hitachi H9000-UHV and the JEM-2000FXV (**Figure 2**). The JEM-2000FXV was initially manufactured to include a cryogenic shield, which was subsequently removed to allow more access to the sample, and in both these instruments the column was modified to maintain a pressure of ~10^{-10} Torr. The timeline in **Figure 2** illustrates the international, incremental, and collaborative nature of UHV-TEM engineering and culminates

in current state-of-the-art UHV-TEM conditions, where high resolution *in situ* TEM data can be obtained at true surface science standards.

3.2 Adding *in situ* capabilities

In addition to maintaining UHV at the sample, the second key consideration for *in situ* UHV-TEM of crystal growth processes is modification of the microscope to allow physical deposition or gas flow inside the column. Installation of a deposition system (either thermal, e-beam, or gas lines) at a port near the sample location enables the user to replicate processes that take place in conventional growth chambers (**Figure 3**). Other strategies include beam-induced deposition via the primary beam, deposition sources integrated on the sample holder, and deposition by DC magnetron sputtering.[84,85] **Figure 3** illustrates some of the variety of instrumentation developed for *in situ* UHV-TEM deposition experiments and we discuss the strategies in more detail below.

3.2.1 In-column deposition

Deposition inside the TEM column can be achieved in many ways. Seminal studies by Pashley *et al.* integrated a Mo wire ring source concentric with the electron beam.[46] This was heated with DC current to avoid electron beam disturbance from oscillating magnetic fields. A manual aperture allowed the deposition time to be controlled. Building on this, Takayanagi and coworkers positioned a thermal evaporator through the top-entry port of the TEM, using the side entry port for the sample.[55] The system included tungsten filaments and crucibles for a variety of metals. Knudsen Mo crucibles,[63] W filaments,[63] and Ta filaments[86] have also been installed in ports for molecular beam epitaxy, and e-beam evaporation systems have been integrated into the column.[28,76] These in-column deposition systems are versatile and capable of replicating essential features of conventional deposition, but require a large effort in microscope modification. Moreover, in the case of e-beam or Joule heated filaments, care must be taken to account for deflection of the electron beam due to stray fields. Attempts to address these issues include the use of electron bombardment evaporators, which use the electron beam from the TEM to aid deposition, and can be easily removed and replaced through the load lock.[87]

In-column gas flow can also be incorporated via capillary tubes that direct the gas close to the sample. This enables semiconductor growth via chemical vapor deposition, for example using disilane or digermane, or gases for oxidation, reduction, and catalytic studies.[18,30,72] A limitation of UHV-TEM instrumentation for gas phase reactions is the relatively low maximum gas pressure (up to ~10^{-5} Torr), since pumping is typically via ion pumps and turbomolecular pumps optimized for lower pressure. For context, ETEMs can typically handle higher gas flows and pressures in the tens or hundreds of mTorr,[38] and up to atmospheric pressures in windowed gas cells.[88] This can be beneficial for *in situ* or *operando* studies of nanomaterial interactions with their ambient working environment. However, the precise control over gas composition, local environment, and sample surface provided by UHV-TEM means that the two techniques are often used in a complementary fashion for gas phase experiments, as discussed further in **Section 5**.

3.2.2 Side chambers

A more flexible strategy for integrating deposition and other capabilities involves the attachment of UHV side chambers to the TEM, with vacuum transfer of the sample between

the side chamber and TEM column. UHV side chambers allow a larger geometric volume for deposition and often include thermal, e-beam, and molecular beam epitaxy evaporators in one system. **Figure 3c** shows an example of a unique side chamber that enables magnetron sputtering.[85] Nanoparticles are created using a DC magnetron sputtering gun in ultraclean Ar, and a pipe inlet allows nanoparticle transfer from the chamber onto the substrate mounted in the objective lens. This equipment has been used to study processes occurring directly after the initial nucleation of nanoparticles, such as sintering, epitaxial reorientation, particle burrowing, and oxidation.[85,89,90]

Side chambers do not meet the full criteria for *in situ* deposition since growth is interrupted and the sample cools down before imaging (in the case of heated depositions). Nevertheless, the sample can be imaged within a few minutes of deposition and without exposure to air. This makes it possible to survey the experimental parameter space without unwanted reaction of the deposited material. Such capabilities generate valuable studies in catalysis and epitaxy due to the UHV environment throughout the deposition and observation process. Side chambers also allow sample preparation, calibration, and further characterization, as will be discussed in **Sections 3.3 and 3.4.**

3.2.3 Holders for in situ UHV-TEM

Sample holders for *in situ* UHV-TEM generally allow sample heating for quantitative exploration of thermodynamic and kinetic mechanisms. Double tilt capabilities are also crucial for optimizing imaging conditions. Holders with both heating and double tilt capabilities are widely available for conventional TEMs but designing such holders to be compatible with UHV-TEM is challenging. In particular, the entire holder must be baked on entering the microscope to remove adsorbed impurities, usually by heating the holder in the loadlock with a lamp or heater tape around the loadlock. When using the holder to heat the sample during the experiment, microfabricated heatable chips provide flexible options for different sample types. Furnace-style heaters, often used in conventional TEM, are usually avoided as the material comprising the furnace may outgas and contaminate the sample during heating. Instead, to minimize the total volume of material that becomes hot, a useful strategy is resistive heating of the sample: derived from strategies for heating in STM, the sample is in the form of a strip, clamped at both ends, and current is flowed through it. This approach works well for samples based on silicon of suitable conductivity, while other materials can be placed in direct contact with silicon to heat in a similar manner.[74]

UHV-TEM holders must also enable reliable sample handling and transfer. This has led to two overall design strategies. The first is based on the side entry holder design common in conventional TEM. A side entry sample rod has the benefit that heat, tilting, and other capabilities such as deposition sources can be actuated easily through the rod and conveniently repaired or reloaded when the holder is removed. An example of a side entry holder designed for UHV-TEM metal deposition is shown in **Figure 3b**.[84] The sample geometry must be designed for the holder, since the direction from which the deposition flux arrives is restricted by the polepiece and holder geometry. This can be limiting if multiple viewing directions are required to form a complete description of the growth kinetics. The most important limitation, however, is that the rod is exposed to air each time a new sample is loaded and any capability, such as deposition on the holder, must be baked each time; furthermore, the sample rod cannot be transferred to attached UHV chambers.

The second sample holder strategy is a detachable cartridge or puck. An example of a cartridge loaded into the microscope from the side is shown in **Figure 1** (bottom right). Top-mount cartridge systems have also been successfully implemented.[53,66] In either case, the sample (possibly already mounted on a small puck) is loaded into a free-standing assembly that is introduced into the vacuum system through a loadlock and then moved between the vacuum chambers and microscope via mechanical transfer rods. Such an arrangement is necessary if the sample is to be transferred into a side chamber for sample preparation and characterization. A disadvantage is the complexity as compared to a side entry holder, since sample tilting, heating and biasing connections must be made in the column rather than through a sample rod. This is discussed further in **Section 5**. However, the mechanical decoupling of the cartridge from the outside world during imaging presents advantages over side entry holder design in terms of decreased thermal drift and influence of external vibrations.

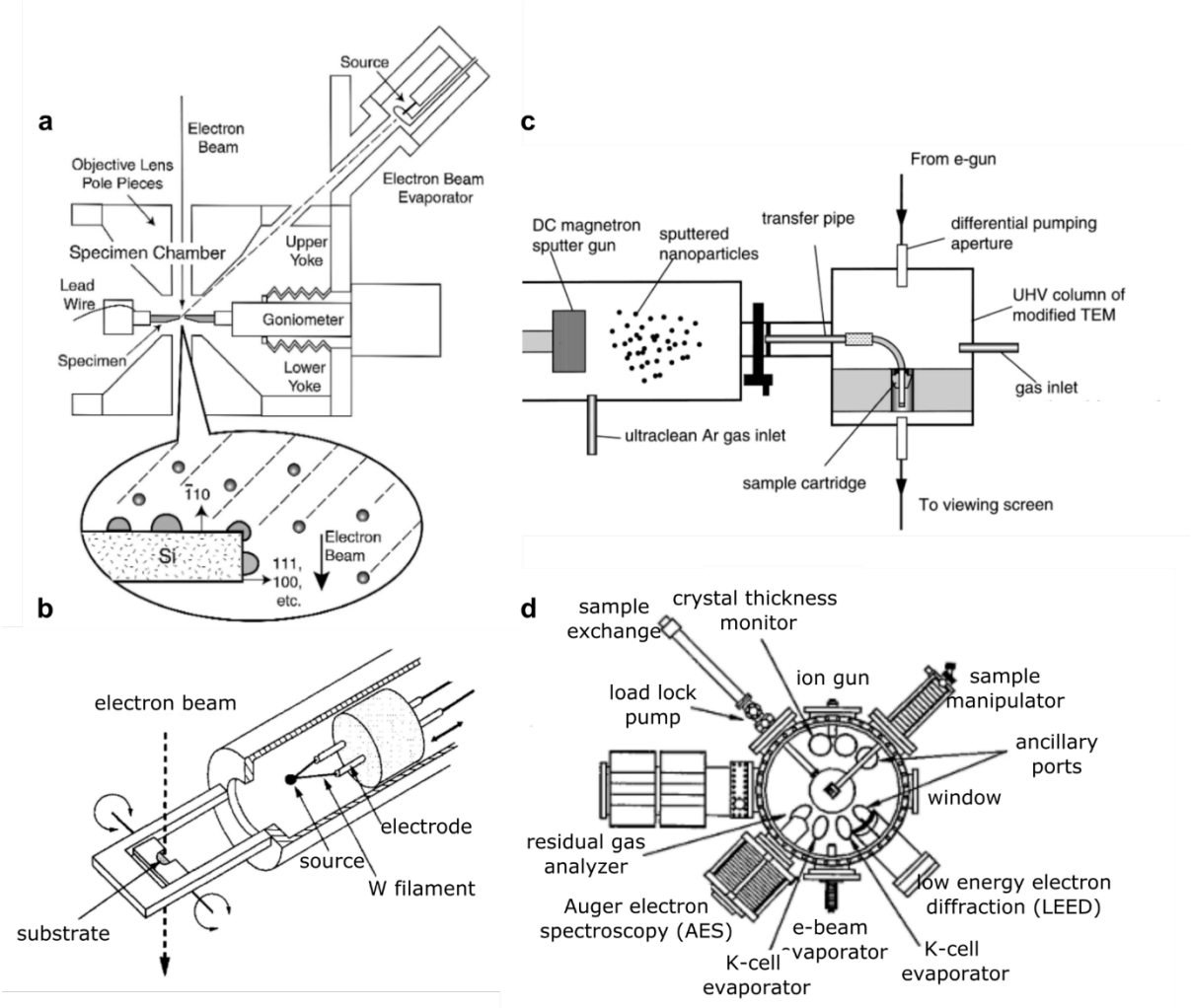

Figure 3: Incorporating *in situ* deposition in the TEM column. a, Cross sectional schematic of in-column *in situ* deposition system that incorporates an e-beam evaporator in a port in the microscope (reproduced from [28], with permission from Elsevier). **b,** Schematic of holder-based *in situ* deposition, with filament heated by electric current (reproduced from [84], with permission from Elsevier) **c,** Cross sectional schematic of side chamber for *in situ* deposition via DC magnetron sputtering (reproduced from [85], with permission from Wiley) **d,** Plan view cross section of the SHEBA system with multiple *in situ* deposition and characterization capabilities inside the electron microscope (reproduced from [74], with permission from AIP).

3.3 Additional functionalities for sample preparation and calibration

As well as the microscope modifications we have discussed that enable UHV conditions and *in situ* deposition, integrating additional functionalities increases the ability of *in situ* UHV-TEM to produce quantitative and transformative information. Examples of such additions are sample surface preparation tools and methods for calibration of temperature or flux, which we discuss in this section, and complementary analytical techniques, which we discuss in the next section. Literature shows that UHV-TEM instruments tend to be customized according to particular research problems of interest, and their functionalities evolve over time as new questions are asked and answered.

To prepare atomically clean substrates, *in situ* vacuum annealing, ion beam milling, and laser cleaning capabilities have been added to ports or side chambers in UHV-TEM systems.[4,57,91] The loadlock offers another location to add such capabilities. A radiant heater is commonly added there for specimen outgassing, but more complex possibilities include a jet of hot gas for cleaning and *in situ* chemical reactions.[66]

Calibration is an essential requirement for interpretable data. To quantify deposition rates, a quartz crystal microbalance (QCM) is typically placed near each evaporator. Post-deposition thickness measurements (Rutherford backscattering, medium energy ion scattering or profilometry) can be used as a calibration to confirm the deposition amount.[86] Systems with multiple effusion cells for compound growth require pre-calibration with quadrupole mass spectrometry to determine the molecular species of the fluxes over the range of effusion cell temperatures.[63] The arrival rates of these molecules can then be monitored by a QCM. Pyrometers and thermocouples may be added to the system to give a quantitative temperature read-out.[66] Temperature measurements are often limited in accuracy, particularly on nanomaterial substrates or substrates with low thermal conductivity where significant temperature gradients occur within the sample.[11] This type of calibration is an area where further development would be beneficial, as we discuss in **Section 5**.

3.4 Integrated UHV fabrication and characterization systems – ‘lab in a microscope’

Although TEM data itself greatly advances our understanding of dynamic crystal growth phenomena, correlation with measurements from other techniques provides a more complete characterization of structure-property relations. Correlative measurements from multiple techniques can be challenging to implement in a consistent manner, particularly for air-sensitive materials. This is mainly due to issues in transferring materials between the fabrication chamber, the electron microscope and other characterization tools. This challenge is addressed by integrating a cluster of complementary deposition and characterization capabilities, along with the TEM, into a single UHV environment, allowing for comprehensive sample preparation and analysis without breaking vacuum.

Aiming to create a fully integrated ‘lab in a microscope’, several UHV side chambers have been developed to add functionalities within the controlled environment. The functionalities include focused ion beam (FIB) irradiation, scanning electron microscopy (SEM), STM, low energy electron diffraction (LEED), XPS, and AES, as well as deposition. They add valuable information to high-resolution TEM analysis when tailored to specific applications. For example, the SPEAR (Surface Preparation Evaluation Analysis Research) system connected to the Hitachi H9000-UHV at Northwestern University included tools for ion bombardment (Ar, O, Xe ion milling), surface characterization (XPS, AES, SEM), and fabrication (MBE,

evaporation) among other capabilities (**Figure 4a**).[35] The side chambers for the Hitachi H9000-UHV at the IBM T. J. Watson Research Center included FIB, SEM, AES, sputtering, optical pyrometry, electron beam and thermal evaporation, with chemical vapor deposition available within the TEM column (**Figure 4b**).[72] The UTSICS (UHV-TEM-STM Integrated Characterization System) in Tsukuba, Japan incorporated a molecular beam epitaxy system, STM, XPS, and sputter ion deposition to enable comprehensive sample growth, preparation, and characterization without breaking vacuum (**Figure 5a**).[75,92] The VG HB501A MIDAS (Microscope for Imaging, Diffraction, and Analysis of Surfaces) at Arizona State University included SEM, AES, RHEED, metal evaporators and a surface magneto-optic Kerr effect station for correlating microscopic structure with macroscopic magnetic properties (**Figure 5b**).[36,93]

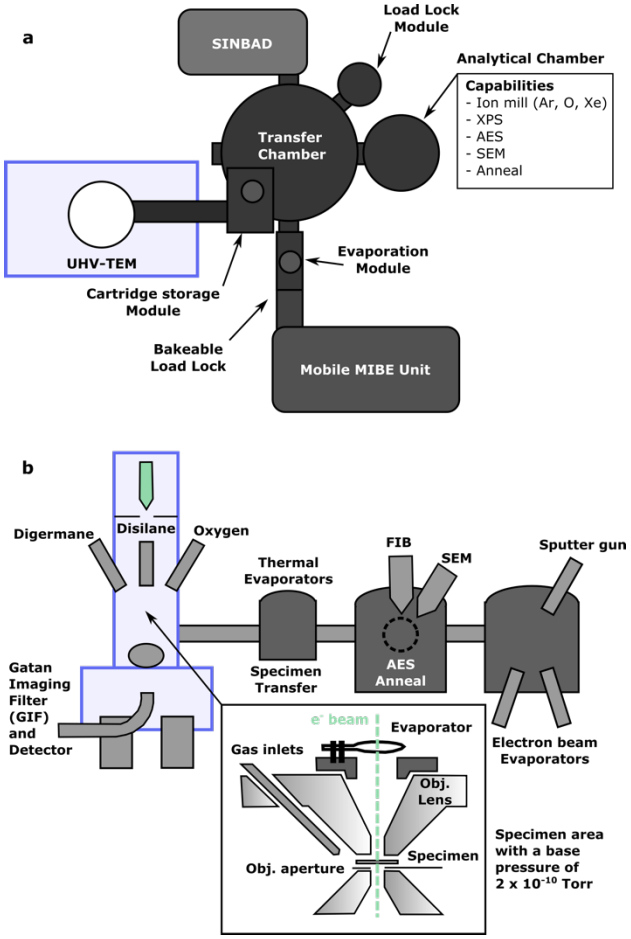

Figure 4: Two examples of customized UHV-TEM deposition and characterization systems. a, Top view schematic of SPEAR system which is based on a Hitachi H9000-UHV instrument and is the first system to integrate magnetron and ion beam deposition techniques (magnetron ion beam epitaxy (MIBE) and stabilizing ion beam epitaxy (SINBAD)).[35] **b,** Side view schematic of the IBM H-9000UHV integrated system optimized for CVD growth in the column and *ex situ* physical deposition and processing.[72] (Images reproduced from [4], with permission from AIP).

Connected side chambers enable vacuum transfer from the microscope to sample preparation and analysis functionalities that cannot (or do not need to) fit within the polepiece. Naturally, the disadvantage is that these processes cannot be observed *in situ.* Furthermore, when adding a side chamber to the TEM, it is essential to minimize pump vibrations or other interference to the electron beam. SHEBA (Surface High energy Electron Beam Apparatus), developed in the 1990s, took a different approach in which all its capabilities - molecular beam epitaxy, ion guns, AES, and LEED – were placed inside the TEM column (**Figure 3d**).[74] Multiple observations were possible *in situ*, but the polepiece gap was expanded to accommodate the set-up, creating a trade-off with resolution, measured at ~10 nm. With over 30 years since the development of SHEBA, advances in aberration correction and vacuum technology are highly encouraging for the continued development of integrated 'lab in a microscope' setups capable

of achieving atomic resolution imaging and high performance spectroscopy. A recent example moving towards this integrated future is CANVAS (Controlled Alteration of Nanomaterials in Vacuum down to the Atomic Scale), that includes a modified Nion UltraSTEM 100 with spectroscopic capabilities, aberration correction, low electron energy (keV) operation, UHV environment and gas flow capabilities, with integrated UHV chambers for evaporation, atomic force microscopy (AFM), laser annealing, and even a glove box for preparation of air-sensitive samples set over two floors (**Figure 5c**).[78] The promise of these developments for the future of *in situ* UHV-TEM is discussed in **Sections 5.4 and 5.5**.

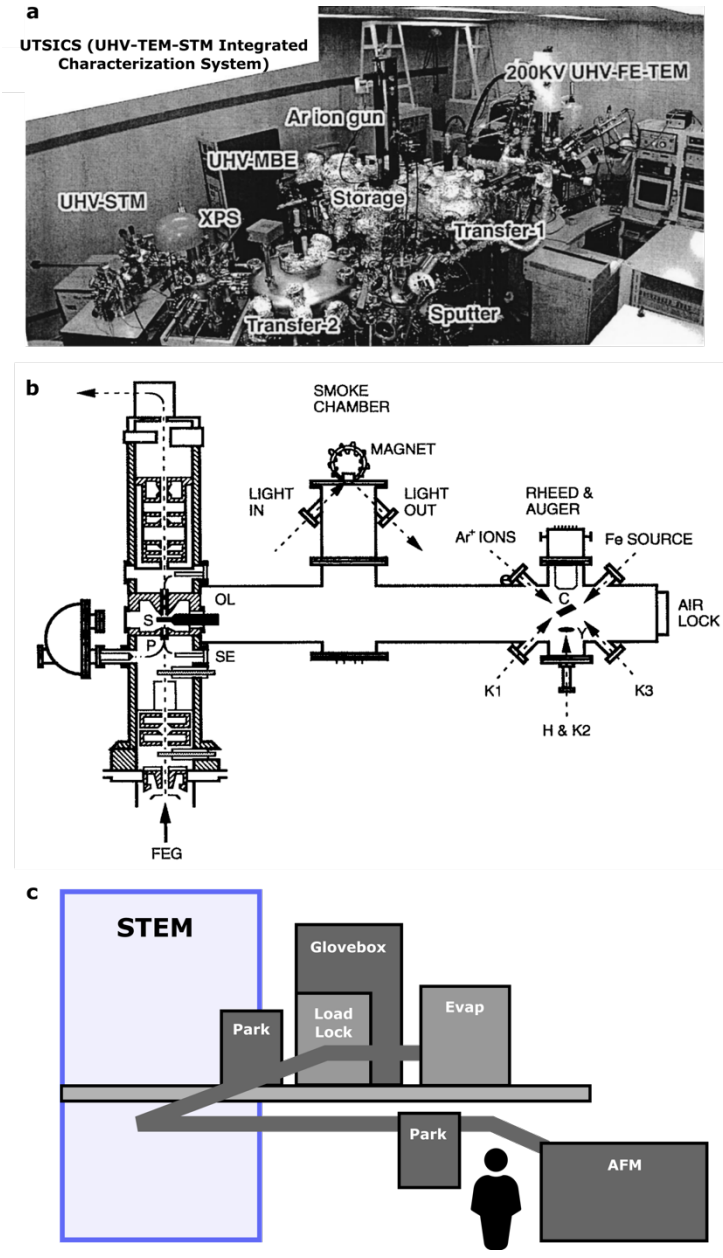

Figure 5: Further examples of integrated UHV-TEM deposition and characterization systems. a, Image of integrated surface analysis and HRTEM/STM system (UTSICS UHV–TEM–STM integrated characterization system) at the National Institute for Materials Research in Tsukuba, Japan.[75] (Image reproduced from [4], with permission from AIP) **b,** Schematic of MIDAS VG HBS01-S column and preparation chamber.[36] In the microscope column are the electron parallelizer (P), secondary electron detector (SE), sample (S), objective lens (OL), and field emission gun (FEG). The specimen preparation chamber consists of a SMOKE chamber for surface magnetism analysis, a cylindrical mirror analyzer (CMA) for AES and RHEED, and sample surface preparation tools such as an Ar^+ ion sputtering gun, and Fe evaporator, a sample heater (IT), and Knudsen cell evaporators (Kl-3). Also shown are the Cu crystal, the YAG crystal (Y), and the air lock for fast sample entry. (Schematic reproduced from [93], with permission of AIP). **c,** Cross-section of CANVAS system: STEM, loadlock and glovebox, evaporation chamber (evap), atomic force microscope (ARM) and sample storage (Park). Schematic adapted from ref. [78]

4. Scientific accomplishments of *in situ* UHV-TEM in crystal growth phenomena

The instrument development described above was motivated by the need for quantitative *in situ* measurements of thermodynamic and kinetic phenomena that could not be obtained with other techniques. In this section, we illustrate some of the scientific contributions of *in situ* UHV-TEM in studying crystal growth phenomena. We focus on studies in the areas of nucleation and growth, thin film homo- and heteroepitaxy, and surface oxide growth. We do not attempt to provide an exhaustive list of all studies undertaken, but aim to showcase the range of dynamic crystal growth phenomena that *in situ* UHV-TEM can address and set the context for discussing future areas of application.

4.1 Nucleation and growth of nanocrystals

In situ UHV-TEM has significantly advanced our understanding of nucleation and growth of nanocrystals on different substrates. By limiting heterogeneous nucleation sites and impurities, and minimizing extraneous reactions and electron-gas interactions during growth, fundamental phenomena such as diffusion, attachment, and strain evolution can be observed. Compared to other spatially resolved surface science techniques, such as STM, TEM offers increased temporal resolution, sensitivity to key properties below the surface, such as the strain fields associated with steps and the structure of domain boundaries, and the ability to observe interfacial or buried structures such as misfit dislocations. *In situ* UHV-TEM is thus particularly useful in elucidating growth modes of nanocrystals where three-dimensional structure plays a role, yielding experimental data to match with quantitative kinetic models.

4.1.1 Nucleation and growth mode: fcc metals on fcc (111) substrates

The power of *in situ* UHV-TEM in nanocrystal nucleation and growth is exemplified by studies of the deposition of various face centered cubic (fcc) metals on (111) surfaces of fcc metals.[8,94–96] The materials studied include metals prone to rapid reaction in ambient conditions, such as Ag and Cu. The resolution afforded by TEM enables small islands and single-layer height surface steps to be observed. This, combined with *in situ* temporal resolution and UHV environment, allows the determination of incubation time and growth mode (Volmer-Weber, Stranski-Krastanov, or Frank-van der Merwe) for direct comparison with classical nucleation theory.

In situ UHV-TEM studies show fcc/fcc-metal growth modes are highly dependent on the material system (**Table 1**). For example, Ag grows on Au(111) in a layer-by-layer Frank-van der Merwe fashion, as evidenced by the time-resolved measurements in **Figure 6a**.[94] In contrast, Cu grows on Au(111) via the Volmer-Weber mode, with triangular nanoislands forming preferentially along domain boundaries.[8] Since the misfit of Cu on Au is -11.4 %, this preferential nucleation is thought to occur due to isotropic contraction of Au at domain boundaries, a mechanism highlighted by *in situ* UHV-TEM.

TEM is well-suited for such studies because moiré and dark field image contrast yield information on growth mode, defects, and strain, even where atomic resolution is not obtained. While bright field imaging in TEM involves direct imaging of the sample using the transmitted electron beam, dark field imaging selectively captures electrons scattered from a specific lattice plane at a certain orientation, revealing features of interest such as misoriented regions, misfit dislocations or strain fields. For example, *in situ* UHV-TEM analysis of the moiré spacing and diffraction pattern of the Au/Pb system accurately detects the nucleation of Au_2Pb monolayers.[95] Au on Pd, on the other hand, nucleates separate dendritic islands instead of forming stoichiometric compounds, and is initially pseudomorphic with no misfit dislocations.[8]

Misfit dislocation density decreases during growth, suggesting some degree of interdiffusion.[95] *In situ* UHV-TEM analysis of the fascinating variety of growth mechanisms, surface structures, and interfacial defects in fcc/fcc-metal growth adds experimental insight to classical nucleation theory. Furthermore, these experiments provide crucial insights to aid the design of metal/metal heterostructures that are widely used as electronic contacts, interconnects, and other device components due to their unique optical, electronic and catalytic properties.[97]

Table 1: Summary of crystal growth phenomena for fcc metals on fcc (111) surfaces. Phase diagram labels: CSS – complete solid solution, OP – ordered phase, MC – metallic compound, IM – immiscible (Table adapted from [8], with permission from Elsevier).

Deposit/Substrate, Temp	Phase Diagram	Results	Ref
Pd/Au, 50-70 ºC	CSS	Interdiffusion	95
Au/Pd, 50-70 ºC	CSS	Monolayer nuclei (dendritic)	8
Pd/Ag, 50-70 ºC	CSS	Dendritic nuclei	8
Ag/Pd, 50-70 ºC	CSS	Monolayer nuclei with misfit dislocations	95
Au/Ag, 50-70 ºC	CSS	2-3 layer-by-layer growth with reconstruction	96
Ag/Au, 190 ºC	CSS	Layer-by-layer	94
Cu/Au, 50-70 ºC	CSS + OP	Nanoisland growth with misfit dislocations	8
Pb/Au, 50-70 ºC	MC	Au_2Pb	95
Au/Pb, 50-70 ºC	MC	'Monolayer' of Au_2Pb	95
Pb/Ag, 50-70 ºC	IM	Monolayer nuclei	8
Ag/Pb, 50-70 ºC	IM	> 10 layer-by-layer growth with misfit dislocations	95

4.1.2 Kinetic modeling: Au on HOPG

In situ UHV-TEM studies can also delve deeper into kinetic models for nucleation and growth. Here, time-resolved data is used to map to analytical models, while UHV allows one to study these processes within a controlled environment. An example is the growth of Au nanocrystals on highly oriented pyrolytic graphite (HOPG).[31,98,99]At low temperatures, large dendritic particles nucleate with low density in areas where the HOPG is clean, while small, rounded particles form with high nucleation density on 'dirty' areas of the HOPG. Without *in situ* studies, it would have been difficult to characterize how these two growth modes arose or measure lateral growth rates as a function of time (**Figure 6b**). Correlation of structural evolution with the size of the adatom capture area within a diffusion-limited growth model resulted in a quantitative estimate for the diffusion barrier for Au on graphite.[31] Higher temperature produced facetted shapes[98] dominated by direct impingement[99] rather than diffusion and capture, as in the low temperature regime. Diffusion lengths and adsorption/ diffusion energies were obtained by matching volume evolution (**Figure 6c**) to a kinetic model including direct impingement and capture. This example highlights the importance of temporal resolution to fit fundamental kinetic models and quantify growth parameters. The measurement of diffusion barriers, diffusion lengths, and energies of adsorption/diffusion illustrated here are possible for many other materials systems using *in situ* UHV-TEM.

4.1.3 Nanoisland growth, sintering, and coalescence: Cu on Cu and metals on van der Waals surfaces

Observation of sintering and coalescence processes during growth and annealing provide a means to understand many thin film phenomena, such as wetting, catalysis, coarsening, and diffusion. *In situ* UHV-TEM provides the clean environments and temporal resolution required to extract mechanistic insights.[85,100–103] For example, *in situ* UHV-TEM studies of the sintering of Cu nanoparticles deposited onto a single crystal Cu substrate shed light on the active mechanisms.[85] Small nanoparticles rotate spontaneously into epitaxial alignment with the

underlying crystal, with neck growth via surface diffusion followed by grain boundary migration. For larger Cu particles, bulk diffusion dominates instead,[85] so the *in situ* measurements elucidate key differences between bulk and nanoscale sintering and coalescence.

Many other studies of thin film coalescence and sintering are possible, particularly when heating capabilities and gas flow are integrated.[100,101] Recent examples explore the epitaxial growth of metals on van der Waals layered (2D) materials such as graphene and transition metal dichalcogenides (**Figure 6d**).[102–105] The weak bonding of the 2D material alters surface interaction and energies compared to covalently bonded or amorphous substrates, resulting in nucleation, growth, epitaxy, diffusion, dewetting, and agglomeration that are markedly different in the two cases. For Au on MoS_2, for example, dewetting and sintering of non-equilibrium island shapes can be observed at relatively low temperatures due to the weak bond between the metal and 2D material (**Figure 6e**).[102] Stable equilibrium shapes are observed at higher temperatures, from which one can extract the metal-2D material interface energy.[102] For Ti on graphene, clusters form initially with a thickness of 1-2 layers and grow into large islands.[103] As well as providing convenient electron-transparent substrates for TEM experimentation, 2D materials play an increasing role as components of electronic and quantum devices. These devices require control of the interfaces with conventional metals and semiconductors, suggesting that fundamental studies of van der Waals interactions will become a new and exciting direction for *in situ* UHV-TEM.

4.1.4 Catalytic growth: vapor-liquid-solid (VLS) semiconducting nanowires

Along with observation of nucleation and growth mechanisms, *in situ* UHV-TEM can aid in developing new ways of fabricating nanocrystals. A benefit of *in situ* experimentation is that the effect of a change in process parameters (temperature, pressure) is visible immediately. Mapping of growth parameters to structure is therefore possible without the need for time-consuming post-growth analysis of multiple samples. Combined with a UHV environment to reduce extraneous influences, the result is an ability to measure the effects of variables such as gaseous environment, material flux, and temperature to isolate specific influences on growth mechanisms and move towards novel growth regimes.

An example is the use of *in situ* UHV-TEM to engineer semiconducting nanowires grown by the vapor-liquid-solid (VLS) mechanism.[82,106–108] VLS-grown semiconducting nanowires exhibit favorable properties for use in nanoelectronic devices such as diodes, transistors, and sensors, as well as in optoelectronics, thermoelectrics, and quantum computing.[109] The ability to exert nanoscale control over structural aspects, such as diameter and doping profile, requires a deep knowledge of growth mechanisms. **Figure 6f** shows *in situ* UHV-TEM imaging of Si nanowires during VLS growth.[82] During the course of the experiment, the AuSi catalyst droplet labelled ‘A’ increases in size while ‘B’ decreases, directly demonstrating the importance of Au diffusion and Ostwald ripening in Si nanowire VLS growth and its influence on length, diameter, and sidewall structure.[82] These, and other insights into the VLS growth mechanism, were possible because of the unique combination of temporal resolution, spatial resolution, and controlled environment enabled by *in situ* UHV-TEM. The UHV environment is particularly important here, given the propensity for Si and other technologically relevant semiconductors to react with ambient gases such as oxygen.[109]

In situ growth experiments also proved useful in designing novel heterostructure nanowires. In **Figure 6g**, switching between two GaAs crystal phases, zinc blende (ZB) and wurtzite (WB), was engineered by altering the growth conditions during *in situ* UHV-TEM observation.[108]

Dark field imaging was used to distinguish the two phases so that switching could be measured as a function of temperature and source flux of trimethylgallium (TMGa) and arsine (AsH_3) directed by two capillaries to the sample area. Measurement of the dynamics of switching via *in situ* UHV-TEM provided the understanding needed to design modulated nanowires that use the different band structures of ZB and WZ crystals for quantum confinement and opto-electronic applications. This type of approach can be extended to materials systems beyond nanowire VLS, including catalytically mediated island and thin film growth.[110]

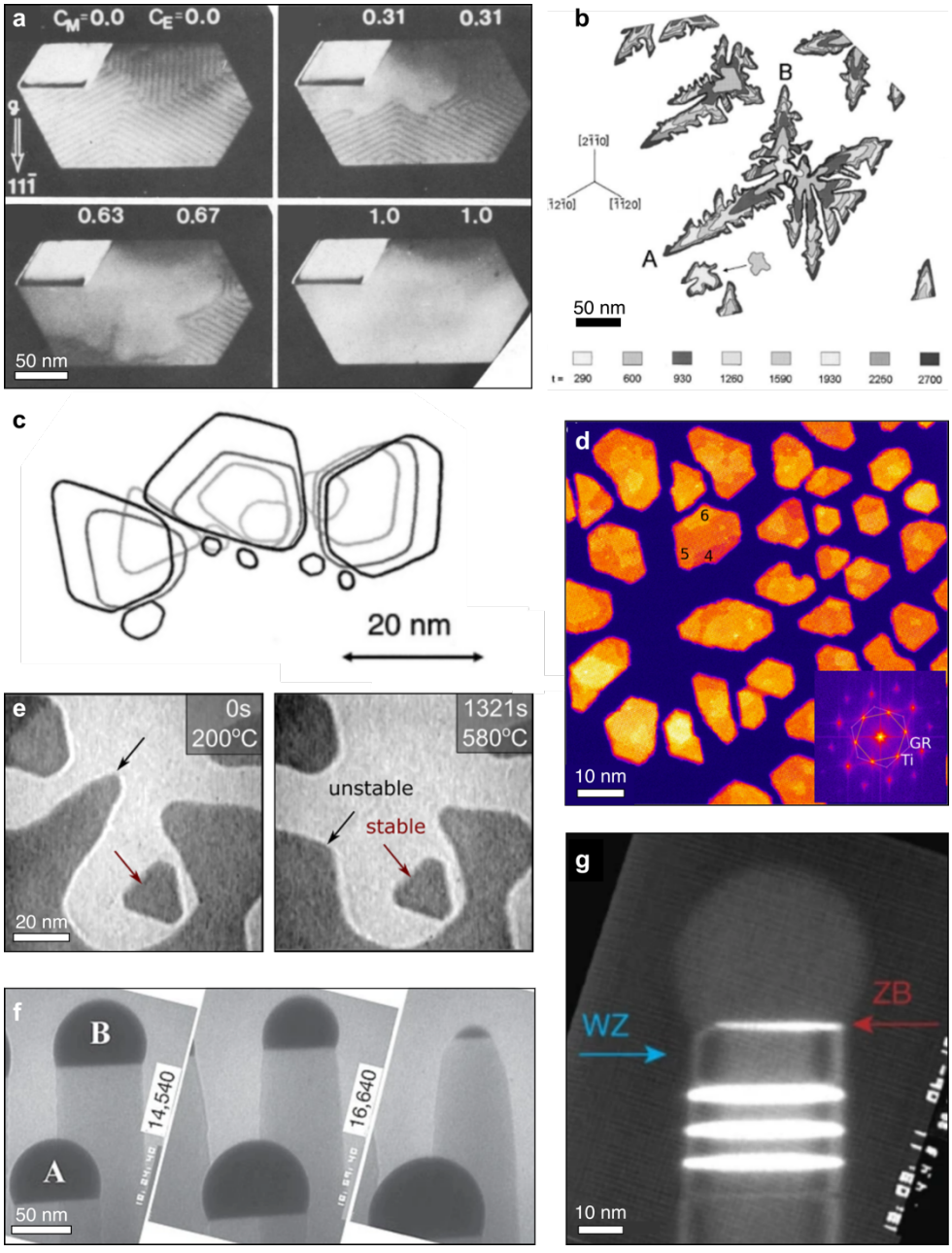

Figure 6: Nucleation and growth of nanocrystals: illustrative examples. a, Layer-by-layer (Frank-van der Merwe) growth of Ag on an Au island (irregular hexagon) at 190 ºC. C_M = amount of Ag deposited with respect to a monolayer, C_E = fractional area covered by Ag monolayer. Ag lifts the Au surface reconstruction, making the fringes disappear.[94] **b,** Contour plots of Au growth on HOPG at room temperature. The dendritic growth rate is high where there is a large capture area ('A') but low when close to a neighbor ('B'). Matching with models

resulted in estimation of the diffusion barrier for Au on graphite at 0.24 eV.[31] **c,** Contour plots of Au growth on HOPG at 350 ºC.[98] Rotation and translation of small particles occurs at the beginning of growth. Matching with models led to values for diffusion length λ (5.8 ± 2.4 nm) and difference in atomic energies of adsorption and diffusion ($E_a - E_d$) = 0.39 ± 0.04 eV. **d,** STEM HAADF image showing layered growth of Ti islands on graphene. Inset Fourier transform shows epitaxy.[103] **e,** Movie stills recorded during heating of Au on MoS_2 from 200 ºC – 580 ºC show dewetting of unstable islands and stable equilibrium geometry.[102] **f,** *In situ* UHV-TEM images recorded during the growth of Si nanowires with AuSi catalyst droplets at 655 °C in 10^{-6} torr disilane. Labels indicate time (in seconds) after the start of growth. Ostwald ripening of Au is visible.[82] **g,** Dark field image of the first zinc blende (ZB) layer that appears on a wurtzite (WZ) GaAs nanowire at 550 ºC after changing AsH_3 and TMGa flow rates. ZB segments appear bright and WZ dark in this imaging condition.[108]

4.2 Thin film homo- and heteroepitaxy

Fundamental mechanisms of thin film epitaxy also benefit from *in situ* UHV-TEM due to the ability to probe the dynamic phenomena associated with each stage of microstructural evolution. The UHV environment is particularly important for semiconductor and metal thin films that oxidize readily. A unique advantage of TEM in thin film growth studies is its ability to obtain both imaging and diffraction information, allowing precise determination of crystal structure and epitaxial orientation. Furthermore, the sensitivity of TEM to strain, such as at dislocations deep within the sample, is helpful given the importance of strain in thin film growth. A full understanding of thin film processing must also include transient effects which occur during heating, exposure to gases, or biasing. Time-consuming or impossible to capture by conventional *ex situ* TEM, these effects are observable *in situ*. Overall, *in situ* UHV-TEM has proven powerful in elucidating phenomena driven by strain, including dislocation introduction, the origin of unexpected epitaxial orientations, and epitaxial growth of reactive materials or on reactive surfaces. We describe several case studies below.

4.2.1 The effects of strain: Ge and SiGe on Si

The growth of Ge and SiGe alloys on Si(001) is a technologically important example where *in situ* UHV-TEM has provided useful insights.[72,111–114] Epitaxial growth of Ge on Si(001) involves a 4% mismatch between Ge and Si and occurs through the Stranski-Krastanov growth mode, in which Ge grows layer-by-layer up to ~3 monolayers, after which islands self-assemble to relieve strain (**Figure 7a, top**).[111] *In situ* UHV-TEM showed that these faceted, coherently strained islands coarsen via surface diffusion of Ge, and the larger islands are bounded by different facets. Misfit dislocations eventually form at the Ge island/Si interface (**Figure 7a, bottom**).[72,115] Understanding the interplay of strain, surface diffusion, surface facet energetics, and dislocation introduction that control Ge/Si(001) strained-layer epitaxy requires measurements that combine sensitivity to strain with temporal resolution. UHV-TEM also enabled the examination of Ge island formation on *in situ* patterned and etched non-planar surfaces, of interest in developing device fabrication strategies.[112] The phenomena observed *in situ*, particularly the evolution of self-assembled quantum dots, are relevant to understanding strained layer growth in other semiconductors. Growth at lower strain, for example for SiGe alloys on Si, favors other pathways for strain relief: a rippled surface or an array of misfit dislocations form as the film exceeds a critical thickness. UHV-TEM enables dislocation introduction to be observed and can help show how dislocations then propagate, even comparing the motion of the same threading dislocation in SiGe before and after the surface has been oxidized.[113]

The power of TEM in resolving buried defects and strain fields makes UHV-TEM well suited for studying other strain-related phenomena in Ge/Si epitaxy. For example, individual misfit dislocations at the SiGe/Si interface influence Ge island nucleation (**Figure 7b**).[72,115] The strain fields of these buried defects extend to the surface and provide a favored environment for nucleation, suggesting opportunities for tailored growth through dislocation and defect engineering. In all of these studies, the strain in thin foil geometries created for TEM study can deviate from the strain conditions in bulk samples, which is something to consider when comparing to bulk phenomena and discussed further in **Section 5.1.3**.

4.2.2 Thin film growth: Fe/Au, Ag/Si, and InSb

UHV-TEM helps to explore thin-film growth phenomena, at and beneath the surface, in materials that would otherwise react with the atmosphere. These materials include technologically relevant metals such as Fe, Ag, In, Pb, Sn, Ti, Ta, Nb, Mo, and Cu,[56,63,93,116,117] and semiconductors, such as Si and Ge, discussed in **Section 4.2.1**. Such studies are particularly useful in nano- and quantum electronics, which rely on metal, insulator, and semiconductor thin film deposition with a high degree of precision in both thickness and properties. An example of a complex growth mode elucidated by *in situ* UHV-TEM is that of Fe on Au(111).[56] *In situ* UHV-TEM studies show that below 0.3 nm thickness, the deposited Fe grows pseudomorphically with the underlying Au substrate. As the thickness is increased to 0.55 nm, misfit dislocations appear at the interface, as expected for conventional Frank-van der Merwe growth. However, at ~1.5 nm the Fe layer undergoes an unexpected transition from the γ to α phase.[56] The *in situ* UHV-TEM observations suggest that the α phase preferentially nucleates on partial misfit dislocation faults. The orientation of the α-Fe/Au(111) film was determined from moiré contrast, displaying both Kurdjumov-Sachs and Nishiyama-Wassermann orientations.[56] Knowledge of these transient phenomena helps in controlling Fe thin film structures.

Deposition on reconstructed surfaces can result in epitaxial film orientations not expected in traditional growth. By utilizing the UHV environment, reconstructed surface structures such as Si(111) 7x7 can be created and maintained for study of deposition. Such experiments show that surface structures formed during the initial stages of metal deposition on Si can alter the epitaxy of subsequently deposited material.[116,118] The importance of controlling such deposition is clear if we consider metal-silicon interfaces in device technologies, where epitaxial orientation can change the Schottky barrier height of Si-metal contacts, Si surface states, and interfacial charge transfer.

As an example, monolayer Ag deposited on the Si(111) 7x7 reconstructed surface can create a commensurate lattice with the Si, resulting in an initial Si(111) $\sqrt{3} \times \sqrt{3}$ -Ag structure (alongside 3x1, 5x2 and other reconstructions possible in the phase space).[116] The Si(111)$\sqrt{3} \times \sqrt{3}$ -Ag structure creates a semiconducting surface state due to the termination of Si dangling bonds by Ag 5s electrons. On further deposition, Ag was expected to grow with its (111) or (110) planes parallel to Si(111). However, UHV-TEM studies instead uncovered two complex and competing epitaxial orientations of Ag thin films on Si(111)$\sqrt{3} \times \sqrt{3}$-Ag (**Figure 7c**).[116] These studies highlight the use of both real and reciprocal space to elucidate structure; the interplay between the two unusual epitaxial orientations could not be explained via *ex situ* studies alone and required *in situ* UHV-TEM monitoring.

Incorporating multiple deposition sources in the microscope allows for the study of compound formation, expanding the range of accessible materials. An example is the homoepitaxial growth of InSb(111).[63] Equal incident fluxes of Sb_4 and In_1 lead to homoepitaxy of InSb leaving an excess of Sb* atoms. These condense at a 'homoepitaxial temperature' T_h, above which homoepitaxial InSb grows with a surface reconstruction, and below which two polycrystalline phases (InSb + Sb) form.[63] Models for adsorption and desorption of Sb molecules match well with experiment, showcasing the applicability of such studies to reactive element and compound thin film formation. Similar *in situ* UHV-TEM analysis could be extended to a wider variety of reactive materials in the future, such as metal and metal chalcogenide growth on the surfaces of alkali halides and layered chalcogenides.[117,119]

4.2.3 Reactive epitaxy: silicide and germanide formation

Metals deposited on Si or Ge often react to form epitaxial or polycrystalline silicides or germanides from the metal-rich end of the phase diagram.[28,76,86,87,120] This process is relevant to formation of the metal-silicide layers used extensively in CMOS technologies at gate, source, and drain electrodes. For example, Pd deposition on Si(111) at 380 ºC forms Pd_2Si islands in a Stranski-Krastanov growth mode, with Pd decorating the Si(111)7x7 reconstruction.[28] *In situ* UHV-TEM can resolve this sub-monolayer deposition by imaging parallel to the interface (**Figure 7d**) – a useful strategy known as profile imaging[121] that is achieved by heating a plan view Si membrane to produce holes with vertical faceted walls. For Pt, *in situ* UHV-TEM shows that deposition on Si(001) at 600 ºC forms a continuous, polycrystalline, epitaxial layer with predominantly PtSi(110)||Si(001) orientation, while at 800 ºC the preferred orientation changes to PtSi(120)||Si(001).[120]

A different growth pathway is displayed by Co when deposited on Si(110): endotaxial (embedded in the substrate) Co_2Si nanowires form, shown post-growth in **Figure 7e**, coherently strained and with a fixed length to width ratio.[87] Time-resolved imaging shows an incubation period after which the Co concentration reaches the solubility limit of Co in Si and nanowires form with length L scaling with $L \sim t^{1/3}$. Co on Si(111) shows different morphology[86] which is described using a thermally activated, facet-dependent growth model.

Reactions with Ge similarly result in epitaxial growth of germanides. Single crystal, self-aligned metal germanides have been studied as a way to minimize grain boundaries and reduce interface roughness for metal-semiconductor contacts. Diffraction patterns obtained during the evaporation of Co onto Ge(001) are compared in **Figure 7f**, showing the continuous epitaxial growth of a thin film of Co_5Ge_7 on heating.[76] On further annealing, this thin film breaks up to form separated nanoislands and relieve strain energy. The kinetics of this process can be monitored *in situ* via bright field imaging and electron diffraction.[76] Due to the high reactivity of the materials involved, *in situ* UHV-TEM is essential in elucidating these mechanisms.

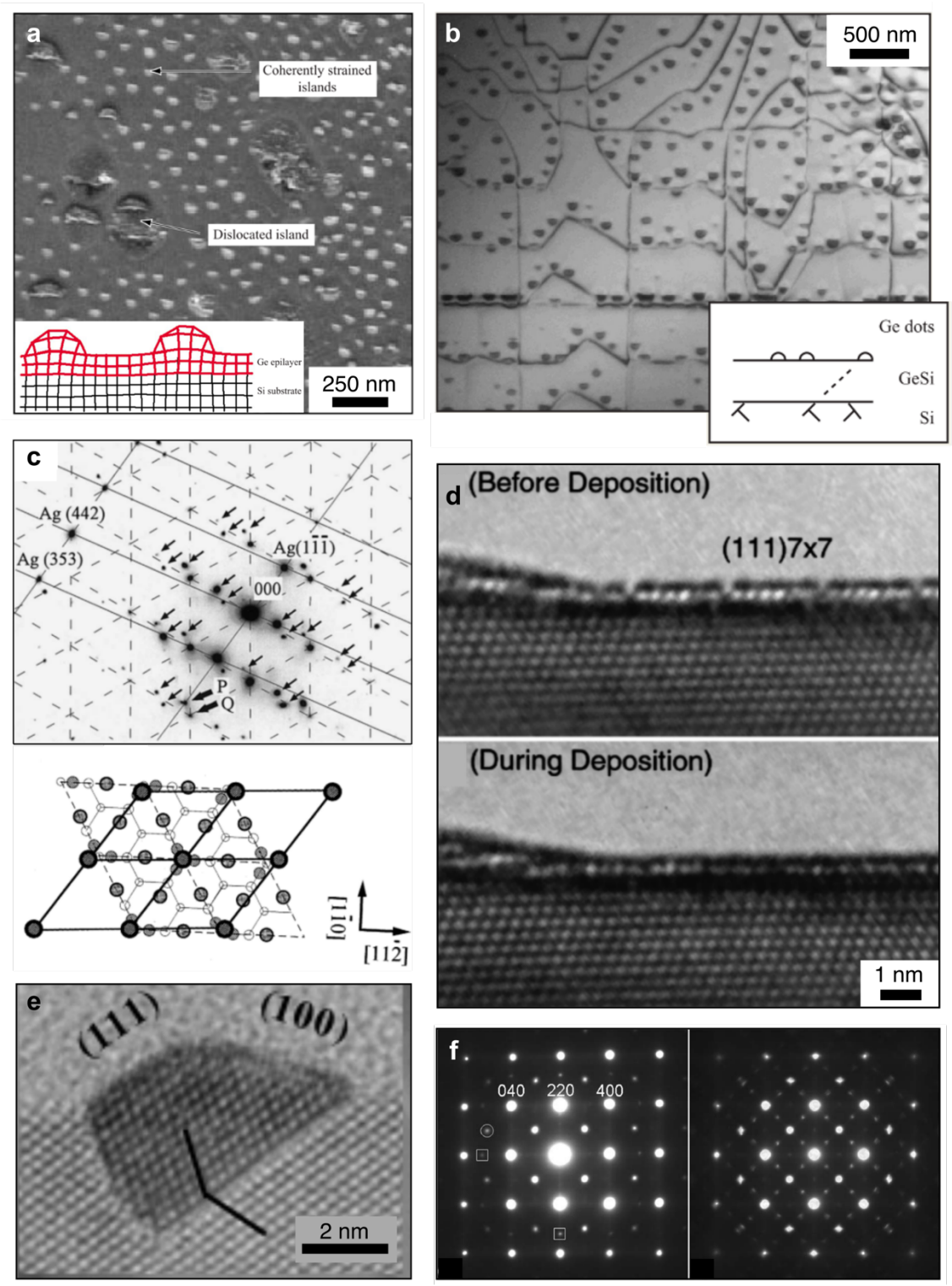

Figure 7: Thin film homo- and heteroepitaxy: illustrative examples a, TEM image showing Ge islands formed after deposition of ~10 ML of Ge on Si(001). Inset: Schematic diagram showing island structure, where strain is relieved as the Ge lattice expands at the tops of the islands.[115] **b,** Ge islands grown on a 300-nm $Si_{0.8}Ge_{0.2}$ alloy layer on a Si substrate. The alloy layer has partially relaxed, forming misfit dislocations at the SiGe/Si interface, and the Ge islands grow in rows associated with these dislocations.[115] **c,** SAED pattern (top) and corresponding atomic model (bottom) of epitaxial alignment for Ag(1$\bar{3}$4) on Si(111)$\sqrt{3} \times \sqrt{3}$ /Ag surface. Shaded lines indicate unit cell of $\sqrt{3} \times \sqrt{3}$ structure, while bold lines show the

Ag($1\bar{3}4$)lattice plane. Ag grows as islands on this surface, with Ag($1\bar{3}4$) epitaxially aligned with Si(111). Another potential growth mode consists of flat striped islands with two separate domains, one commensurate with the Si(111)$\sqrt{3} \times \sqrt{3}$-Ag lattice, and the other with a 5% mismatch. The interplay between these configurations can be distinguished via SAED.[116] **d,** Profile imaging of Si(111) surface before deposition (top) showing the Si(111) 7x7 reconstruction, and during Pd deposition (bottom) where the reconstruction is replaced by thin layer of Pd_2Si.[28] **e,** Post-growth cross-sectional TEM image of endotaxial Co_2Si nanowire grown in UHV-TEM.[87] **f,** SAED patterns showing Co film deposited on Ge (001) after annealing at 225 ºC (left) and 300 ºC (right). The diffraction pattern changes gradually on heating, indicating a transformation of hcp-Co and reaction to form Co_5Ge_7.[76]

4.3 Oxide formation and other gas phase reactive growth processes

UHV conditions are helpful in obtaining quantitative data regarding crystal growth processes that occur via reaction with a supplied gas. The most obvious example is the growth of oxides, which may form nanocrystals or crystalline or amorphous thin films. *In situ* UHV-TEM offers unique insights into such processes via continuous monitoring of nucleation and growth dynamics. Compared to ETEM, a lower pressure range is accessible but with greatly reduced trace levels of impurities that may otherwise affect surface structure, energy, and behavior.

Experimentally, the procedure is to prepare the starting surface (say by rapid heating, chemical reactions or sputtering and annealing), set the reaction temperature, and inject gases. The structure of the initial surface, as formed, is of course of great importance in itself, and the use of UHV-TEM techniques to measure such surface structures is discussed in detail elsewhere[19,20] and is outside the scope of this review. However, the remarkable results accomplished to date clearly show that UHV-TEM is a powerful tool in surface science, yielding data complementary to that from LEED and STM. For example, UHV-TEM established that surface reconstructions can involve multiple atomic layers at and below the surface, as demonstrated in measuring the atomic positions in the Si 7x7 surface reconstruction.[22,122–126] We anticipate that UHV-TEM will continue to play an important role in quantifying surface structures, particularly when combined with other surface science techniques, as discussed in **Section 5**.

Returning to crystal growth phenomena, an example of the level of analysis possible is shown by studies of Cu oxidation.[30] To prepare the initial clean surface, annealing in methanol vapor at elevated temperature *in situ* is used to reduce Cu oxide to metal.[30] Quantification of Cu_2O nucleation and growth kinetics during oxygen exposure then allows the relative effects of oxygen surface diffusion and direct impingement to be measured (**Figure 8a**).[30] The benefits of *in situ* UHV-TEM include temporal resolution and the ability to observe buried interfaces to determine the 3D structure of the islands (**Figure 8a, inset**). *In situ* UHV-TEM has also provided insight into the complex 3D structures formed by the oxidation of Cu alloys,[127] and has been used to complement higher pressure ETEM experiments.[128] Semiconductor oxidation can also be studied, such as oxidation of Si below 800 ºC which forms a planar oxide. Analysis of image contrast and buried interfacial step positions during *in situ* UHV-TEM oxygen exposure shows that Si oxidation occurs by reaction of terrace atoms rather than those at step edges.[129,130]

A benefit of *in situ* UHV-TEM (compared to say STM) for oxide growth experiments is that it can probe reactions below the surface in nanomaterials of complex morphology, measuring the dependence of the oxide growth reaction on the local geometry of the material. As an example,

the oxidation of indium particles deposited onto a graphene support is shown in **Figure 8b**.[79] This was carried out 'quasi' *in situ*, with In deposition in a UHV side chamber and controlled exposure to ambient air for oxidation. These experiments visualized formation of the interface between oxide and the 2D substrate,[79] and suggest that UHV-TEM has exciting prospects for examining analogous growth reactions in a variety of nanomaterial interfaces. A greater variety of gaseous environments is also possible, as discussed further in **Section 5**. Reactions such as oxidation, reduction, and CO_2 hydrogenation are currently carried out predominantly in ETEM.[131–134] Comparing with observations made in UHV environments, even though at limited pressure, could add a wealth of knowledge in situations that require a reconstructed catalyst surface or a highly controlled gas composition.

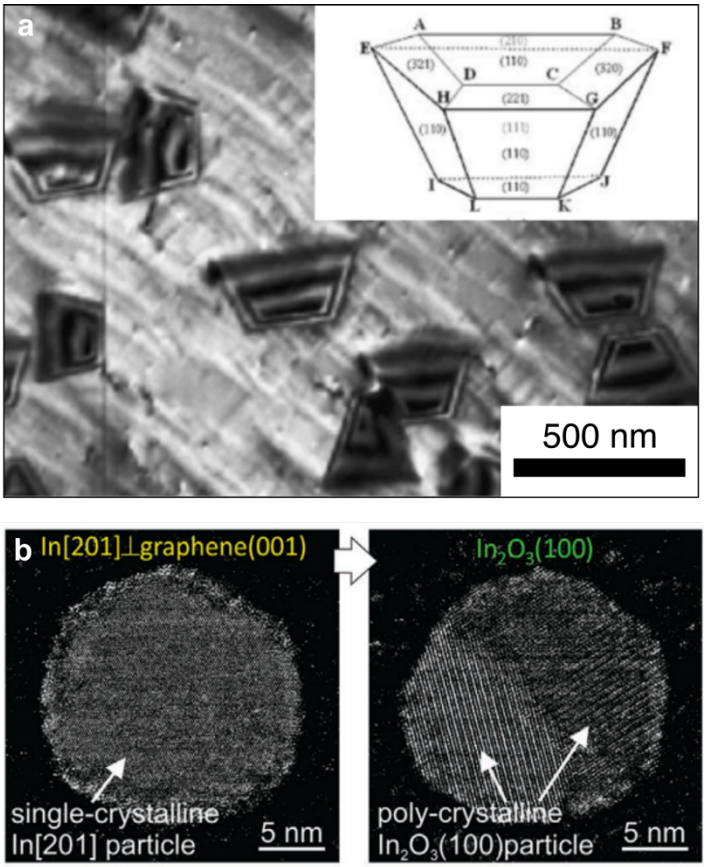

Figure 8: Nucleation and growth of oxides: illustrative examples. A, Dark field images of oxide islands on a Cu(110) surface, cleaned by exposure to 5 x 10^{-5} Torr methanol at 350 ºC then thermally roughened by heating to 750 ºC and exposed to 5 x 10^{-4} Torr oxygen. Inset shows the 3D structure of the resulting oxide crystal.[30] **b,** UHV-STEM images of In particles on graphene as deposited in UHV (left panel), after oxidation in air at room temperature for 24 h (middle panel) and after additional heating in air at 100 °C for 45 min (right panel).[79]

5. Challenges, Opportunities, and Future Perspectives

The studies outlined above illustrate the power of *in situ* UHV-TEM to solve materials problems involving crystal growth. Dramatic instrumental and computational advances have energized the entire microscopy community in recent years and we anticipate that these innovations will be fully adopted into *in situ* UHV-TEM in the future. This will enable measurement of phenomena such as phase transformations, nucleation and growth, site selective deposition, and interface structure with ever more precise imaging and analysis

capabilities and under increasingly better-controlled conditions. *In situ* UHV-TEM will also expand its scope to address other grand challenges in materials design, such as imaging catalytic reaction pathways on surfaces, structure-property correlations in quantum materials, and the behavior of individual defects.

As we envision the future of *in situ* UHV-TEM, it is clear that the opportunities are exciting but challenges and limitations of the technique will remain. Some of the challenges are common to all *in situ* TEM techniques, such as understanding and mitigating electron beam and thin foil effects, and optimizing experimental throughput and data handling. Other limitations are unique to UHV-TEM, including the so-called 'pressure gap' (**Section 5.1.2**), calibration of local temperature and pressure, and developing user-friendly technology given the complexity of UHV conditions and capabilities such as side chambers. Considering the historical evolution of the field, as discussed in **Section 3**, advances in *in situ* UHV-TEM will likely result from a collaborative effort between microscope manufacturers who provide universal requirements such as imaging and spectroscopy, and individual research labs that focus on specialized applications involving aspects such as deposition or sample handling. **Figure 9** categorizes the challenges, opportunities, and future perspectives we see for *in situ* UHV-TEM into four areas: (1) quantification of sample conditions and environment, (2) data collection and analysis, (3) structure-property relations and modeling, and (4) advances in instrumentation. We describe our opinions in these areas in the sections below.

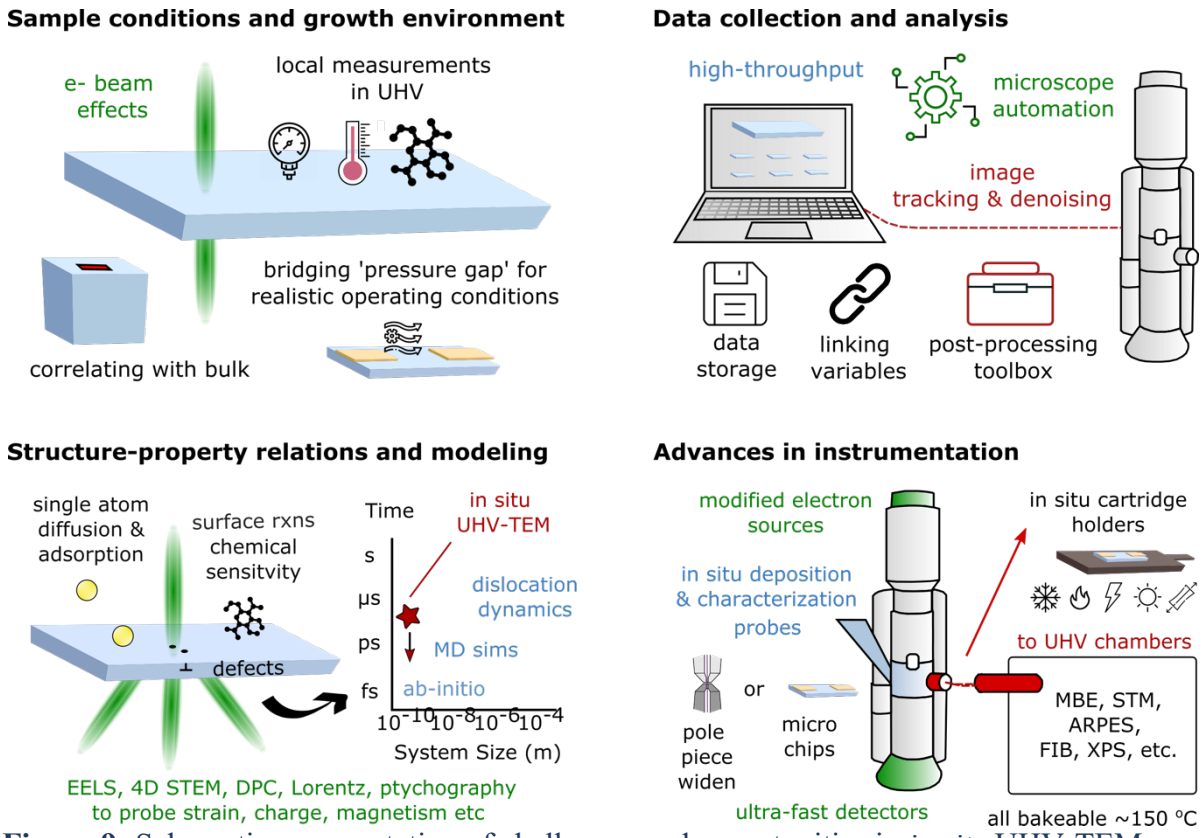

Figure 9: Schematic representation of challenges and opportunities in *in situ* UHV-TEM development.

5.1. Quantification of sample conditions and growth environment

It is important to ensure that the *in situ* experiment accurately represents the problem that we wish to solve – and if it does not, we need to understand the ways in which it differs. This fundamental issue motivates us to consider several aspects of an *in situ* growth experiment:

how the sample geometry (especially the thickness) affects the process under investigation; how the sample is affected by the imaging radiation; the extent to which experimental parameters can be replicated within the microscope, and the accuracy with which we know the local conditions.

5.1.1 Electron beam effects

In any TEM observation the electron beam can damage the sample or modify its surface, complicating meaningful analysis. Irradiation during *in situ* UHV-TEM may cause direct knock-on damage, ionization damage (radiolysis), localized heating, or electrostatic charging.[135,136] Other effects known in conventional microscopy, in particular electron-beam induced deposition of carbon (EBID), are reduced in UHV-TEM, offering a strong advantage when studying *in situ* growth.

Knock-on damage,[7,137] in which atomic vacancies are created by energy transfer from the beam, may be particularly important in growth experiments. Once the sample is imaged at high electron energy, induced defects may influence the next deposition or characterization step. A potential solution is to utilize indexed TEM grids such that only one area of the sample is imaged in each step, which can then be compared with a pristine area. Ionization reactions, which may be more pronounced at low electron energy, require particular consideration during *in situ* UHV-TEM studies in gaseous environments, and efforts have been made to account for the beam-gas interaction numerically.[136–138]. Repeating the experiment at varying electron dose, dose rate or electron energy is useful to monitor the effect of the beam on the gas species and reactants. Localized heating via energy transfer from the beam may raise the temperature by only a few degrees, but may be more significant if the sample has poor thermal conductivity. Electrostatic charging may influence *in situ* experiments involving insulating materials. Pre-coating the TEM grid with a conducting film (Au or other metal to avoid carbonaceous contamination) is not always possible without altering the outcome of the growth experiment, therefore low dose rate imaging coupled with data post-processing may help minimize charging artifacts.[139]

As well as conventional sample damage, electron-sample interactions can influence nucleation, diffusion, and surface reactions in *in situ* UHV-TEM. Diffusion can be enhanced under the electron beam, and crystals are prone to decomposition.[55] Beam effects can be evaluated by performing 'in beam' vs 'out of beam' image comparisons.[18] Operating the TEM at different electron energy (e.g. 30-100 keV) and the lowest possible dose needed for the required resolution and image acquisition rate is good practice to mitigate beam damage and extraneous reactions.[11] Low electron energy (< 60 keV) imaging involves a tradeoff in spatial resolution, while low dose imaging reduces the signal to noise ratio, especially in time-resolved data.[11] With the advent of aberration correction, sensitive detectors, and computational resources,[140] the feasibility of low electron energy, lower dose, *in situ* UHV-TEM moves further within reach.

Despite these technological advances, electron beam effects will continue to require careful consideration for *in situ* UHV-TEM. Current best practices for general *in situ* experiments, enumerated in a workshop at the National Institute of Science and Technology,[11] include obtaining a dose measurement (both dose rate and total electron dose) for each experiment, for example with a Faraday cup; performing a systematic study of the effect of electron dose and energy on each new material studied; reporting total electron dose in publications and presentations; educating new users on the importance of electron beam interactions; and

creating an open database to report the optimal electron dose for specific materials systems.[11] Faraday cup design and measurements inside the electron microscope should also be considered carefully here, in order to accurately account for backscattering and secondary electron emission losses. By adhering to these best practices and continually refining experimental techniques, researchers can better understand and control electron beam effects in *in situ* UHV-TEM experiments.

5.1.2 Bridging the 'pressure gap'

While UHV conditions are essential to achieving fundamental mechanistic insights in ultra-clean environments, real-world processes occur at higher pressures. Pressure dependence can be complex, making it difficult to extrapolate data obtained at UHV to higher pressure ranges. Combining UHV-TEM data with that from higher pressure experiments in ETEM or in a closed gas cell helps to bridge this pressure gap.[141,142] A closed gas cell experiment can reach pressures up to or exceeding atmospheric, and offers other benefits discussed below in **Section 5.1.4**. However, the presence of the windows reduces image resolution and hinders the use of techniques such as EDS. We therefore propose a somewhat different strategy for achieving higher pressure in a UHV instrument, based on environmental SEM techniques: this is to use a semi-closed cell where gas is supplied through the holder to a sample between chips whose windows contain apertures.[143] Compared to a fully-enclosed gas cell, the semi-closed cell offers better resolution and the ability to collect analytical signals; furthermore, we expect that UHV sample preparation can be achieved more readily. UHV-TEM can also be combined with other *in situ* time-resolved studies, such as XPS, that probe growth and catalytic activity at varying pressures.[25,144] This allows insights gained via *in situ* UHV-TEM to be extended more rigorously to higher pressure conditions.

5.1.3 Thin foil effects

In thick samples, multiple scattering, inelastic scattering, and chromatic aberration limit the image resolution, so thin samples (often far below < 200 nm) are used for high resolution analysis. However, growth phenomena involving strain, diffusion, and defects can differ considerably between thin samples and bulk.[145,146] Sample preparation techniques used to create thin films and cross sections from bulk materials, such as focused ion beam (FIB) milling and mechanical polishing, also alter the sample from its pristine configuration. Therefore, care is needed in extrapolating thin-foil observations in *in situ* UHV-TEM to the bulk phenomenon.

Detailed materials modeling coupled with image simulations can help quantify the influence of strain fields and defects. Moreover, correlating UHV-TEM with analysis techniques that allow imaging of a larger area (e.g. *in situ* SEM), the surface of a bulk sample (e.g. *in situ* AFM and STM), or larger scale properties (e.g. optical spectroscopy or magnetic measurements) can enable more accurate extrapolation to macroscopic behavior. These forms of characterization may be integrated within UHV side chambers.[75,78,93]

5.1.4 Measuring the local environment

Accurate measurement of the conditions at the sample is essential to obtain quantitative thermodynamic and kinetic information from *in situ* UHV-TEM experiments. For example, the local gas pressure, composition, temperature, and electric/magnetic fields are required to match *in situ* UHV-TEM data with accurate models.

In the highly controlled environment of UHV-TEM for nucleation and growth studies, even ± 5 °C can have an impact, making precise read-out of local temperature crucial. Calibration prior to the experiment using a pyrometer may not provide the required accuracy. If the sample is supported on a microelectromechanical (MEMS) chip with a heater element, the temperature-current characteristic can be calibrated for one chip and is usually reliable for others fabricated in the same batch.[147,148] However, for samples without local heater elements, or samples whose temperature is affected by the proximity of an *in situ* deposition source or gas environment, it is useful to have a local measurement of temperature at the sample area. For certain materials, local temperature measurements can be performed by EELS using the temperature-sensitive plasmon peak position,[149] the gain and loss phonon peaks in the electron energy spectrum,[150] or the measurement of strobe (noise) peak in EDS spectra.[151] Thermal diffuse scattering in STEM nanodiffraction patterns can also estimate local temperature.[152] *In situ* temperature mapping using such methods, combined with numerical modeling to account for resistive heating with radiation and gas conduction losses, will improve accuracy for *in situ* UHV-TEM experiments. Accurate measurement at cryogenic temperatures is also required for magnetic and superconducting phase transitions that depend sensitively on temperatures in the few-Kelvin range. Integrating miniature thermocouples or other measurement facilities directly into the sample area is possible, although may require more engineering in UHV-TEMs due to the requirements for all materials to be bakeable.

Local pressure and composition measurements at the sample are also necessary in experiments that benefit from precise control of gas or deposition flux partial pressures. In a typical UHV-TEM, the gas pressure is measured by ion gauges, but these are some distance from the sample. There can also be a time lag between gas input, measurement, and equilibrium gas pressure at the sample, as well as a dependence on sample tilt and geometry. Gas analysis via a residual gas analyzer (RGA) or mass spectrometer connected to the UHV-TEM column similarly may not accurately reflect the local gas composition. Closed gas flow cells with electron transparent membranes allow more accurate pressure measurement and have been integrated in conventional TEMs and ETEMs.[142,153,154] Closed cells also can allow integrated RGAs for more accurate gas composition, particularly important in catalysis experiments. Assembling a closed cell in UHV conditions without contamination is challenging, and the sealing systems and membrane windows are susceptible to pressure leakage (further discussed in **Section 5.4.1**). Therefore, the semi-closed cells proposed in **Section 5.1.2** may prove beneficial. We also suggest that including temperature-compliant capacitive MEMS pressure sensors into a heating MEMS chip may be a path forward to achieve local pressure measurement in UHV-TEM growth experiments.[155,156]

5.2 Data collection and analysis

5.2.1 Microscope operation and automation

In situ UHV microscopy is labor intensive, requiring expertise in specialized equipment, particularly with manually operated sample transfers, gas systems, and side chambers. Broadening the application of *in situ* UHV-TEM involves improving ease of use, starting with automated alignment procedures and software controls for apertures and camera operation. Recent advances in automating image capture, alignment, and microscope operation are helpful for obtaining statistically relevant data-sets, drift correction, or conducting *in situ* experiments remotely over long periods of time.[157–160] The field of cryo-EM has for a long time capitalized on many of these opportunities, and *in situ* UHV-TEM microscopists have a lot to gain from the cryo-EM community's experience with automation.[161,162]

Automated sample preparation, transfer, and loading mechanisms could revolutionize the capabilities of integrated UHV chambers, allowing characterization via multiple techniques on the same sample. For example, a bulk sample could be fabricated in an MBE chamber, afterwards obtaining an automatic FIB cross section (as already implemented in the semiconductor industry[163]) to characterize in STEM; the bulk sample could then be moved to connected chambers where correlated properties could be measured: one can imagine UHV-connected optical spectroscopy, micro-probe measurements, or NV magnetometry.

5.2.2 High throughput materials design and testing

Novel computational methods have enabled high-throughput screening of materials with interesting properties. Similarly, efficient growth and characterization of materials are expected to enable novel advances and breakthroughs in materials research. The UHV-TEM environment provides an ideal playground for high-throughput materials design through combinatorial and automated experimentation. For example, one could imagine performing *in situ* growth while systematically varying the deposition temperature, flux rate, or proximity to the source. We are particularly enthusiastic about exploring the opportunities arising from the design of versatile microfabricated TEM substrates, for example with multiple heating elements, to probe parameter space during a single experiment. Moreover, with the automation capabilities and side chambers described above, automated sample loading, processing, feature identification, image capture, and property measurement would allow full sample characterization to be performed overnight or remotely.

5.2.3 Data handling and low-dose imaging

The advent of 'big data' handling and systematic data extraction presents opportunities for the *in situ* UHV-TEM community. Acquiring high pixel-count images at rates capable of resolving atomic scale kinetics pose a challenge that is understood for conventional TEM but relatively new for *in situ* UHV-TEM in statistical analysis of vast amounts of data. A single experiment can produce terabytes of data in several minutes[164] driving a need for increased file storage and transfer capabilities, as well as automated analysis. Most *in situ* experiments shown in **Section 4** were analyzed by hand, which is both time consuming and error-prone. Even if data such as growth rate or defect structure can be obtained for a single nanostructure, the corresponding materials characteristics such as resistance, optical, or magnetic properties represent a statistical average of multiple nanostructures. Repeated analysis is necessary, either over an interval of time or over an ensemble of structures, to obtain statistically significant information.

Low-dose (both dose rate and total electron dose) imaging and real-time denoising are also particularly useful in *in situ* UHV-TEM, where single atom diffusion, surface structure, or catalytic reaction pathways are sensitive to the electron beam. Advances in this area include image tracking and deep learning algorithms, which show great promise for dose-efficient image and video analysis.[164–166] Real-time processing of raw data will allow targeting of specific sample areas, rapid experimental feedback on a statistically significant sample size, and denoising of low signal to noise (SNR) data during the experiment. These computational advances are complemented by hybrid pixel detectors and detectors which count individual electrons, and improved EELS measurements.[167,168] Finally, strategies already implemented to optimize the scanning pattern will increase scanning speed and minimize dose.[169]

5.2.4 Combining multiple data streams

The ability to link variables such as pressure, temperature, and gas flow to the output image stream underpins much of *in situ* experimentation. This must include consideration of temperature and pressure lag and local measurement at the sample area, as discussed in **Section 5.1.4**. *In situ* UHV-TEM also benefits from correlating information from different modes of operation, as shown in the examples in **Section 4** that combined bright and dark field imaging, diffraction and high-resolution imaging. Other modes, particularly EELS, are not yet heavily used for *in situ* UHV growth and deposition experiments, often due to acquisition time. 4D STEM data acquisition, where a full diffraction pattern is collected at every pixel location, is another area of opportunity. Although relatively slow to acquire compared to *in situ* TEM data, one can reconstruct bright field, dark field, differential phase contrast, and diffraction images from a single dataset to visualize specific features of the process under study.[170] Further advanced STEM techniques relevant to UHV phenomena are explored in **Section 5.3**.

Given these multiple, simultaneous data streams, it is challenging for one operator to handle the microscope and control the *in situ* parameters, especially when the material change occurs on short time scales. Software and detector designs that simplify integrated imaging, spectroscopy and other data streams will increase the practical possibilities available with *in situ* UHV-TEM.[11] Moreover, the number of imaging and sample parameters makes it difficult for a single operator to maximize efficiency; parallel simulations or machine learning input may help select the imaging mode and parameters that optimize speed and information content to create an efficient imaging pipeline depending on the information desired.[164]

5.2.5 Post-processing and analysis toolbox

An open-source processing and analysis toolbox for the *in situ* TEM community, like those currently existing for the 4D STEM community (py4DSTEM)[171] and the EELS/EDS community (HyperSpy)[172] could accelerate the wider adoption of sophisticated and reproducible *in situ* UHV-TEM analysis. Many of the important features - automated scripts for drift correction, edge detection, particle growth, particle tracking, crystallographic analysis, adding time increments and process parameters to videos, pattern recognition, and kinetic modeling – are relevant to all types of *in situ* experiments. Generalized image and video analysis Python toolboxes already exist, such as OpenCV library for computer vision, machine learning, and image processing.[173] Although researchers can tailor these toolboxes to their individual needs, a dedicated toolbox with notebook examples would reduce the learning curve for newcomers to *in situ* UHV-TEM and standardize analysis procedures. Moreover, software that incorporates correlative mapping and alignment would allow data obtained via multiple techniques (for example TEM and scanning probe measurements[174]) to be correlated after acquisition from the same area of the sample.

5.3 Structure-property relations and modeling

5.3.1 Specialized imaging modes in UHV

The variety of data acquisition modes in TEM and STEM is expanding rapidly, with innovations in techniques such as Lorentz TEM,[175] holography,[176] ptychography,[177,178] differential phase contrast (DPC),[179] and 4D STEM.[180] If used in UHV, these would unlock numerous opportunities to obtain information on properties and processes. For instance, Lorentz TEM, holography, DPC, and 4D STEM, as used in instruments with conventional vacuum, allow quantitative studies of magnetic textures, electric fields, and strain. These

techniques have provided detailed information on the structure-property relationships in multiferroic materials, such as ferromagnetic shape memory alloys,[181] magnetic domain structures under an applied *in situ* magnetic field,[181] and skyrmions.[182] UHV will enable measurement of these phenomena in materials only a few atoms thick, grown or cleaned *in situ* to give control over surface chemistry. One could envisage cooling at intervals during the growth of magnetic films or structures to image magnetic domains without surface contamination, even resolving the magnetic moments of individual atoms.[183]

Other promising applications for specialized imaging techniques in UHV are the measurement of defect formation and motion, and even the diffusion of individual atoms within the bulk of a material or at buried interfaces. Ptychography provides three-dimensional information;[177] applying this technique *in situ* could provide an outstanding view of deposition, surface reactions, and defect and property evolution under controlled UHV conditions. Moreover, techniques that incorporate image reconstruction, such as exit wave reconstruction and ptychography, can enable low dose imaging.[184–186] Although ptychographic imaging and 4D STEM will expand the reach of *in situ* UHV-TEM, they are less suitable for measuring rapid atom dynamics due to their limited temporal resolution, and will require advances in detectors and readout speeds.

5.3.2 Spectroscopy and energy filtered imaging in UHV

Since the early development of the VG microscopes, it has been recognized that spectroscopic capabilities within a UHV environment greatly benefit *in situ* experiments and provide opportunities for improved measurements on static samples. The utility of EELS, EDS and EFTEM[187–189] *in situ* is shown, for example, in measurements of gas composition,[190] the valence state of metallic nanoparticles,[191] chemical composition of beam-sensitive battery materials[192] and time dependence of catalyst composition.[193] *In situ* TEM combined with EELS is particularly important in the study of solid-state energy devices including batteries, solar cells, and solid-oxide fuel cells.[12] In UHV, such capabilities would greatly improve our understanding of diffusion and phase transformations, the formation and dynamics of surface reconstructions, and segregation during growth. We can also envision measurements of phonon excitations, inter- and intraband transitions, plasmon excitations, and chemical composition[79,194] in UHV-TEMs with integrated EFTEM and EELS capabilities.

Integrating spectroscopic capabilities with UHV has another advantage: minimizing contaminant buildup or extraneous reactions during the long acquisition times needed for compositional analysis. The processes that drive sample contamination in conventional TEM vacuum - electron beam-induced motion and deposition of carbon - are reduced in UHV conditions due to a cleaner sample surface and less contamination from background gases.[195] For beam-surface interactions, the importance of a clean sample surface is known from experiments in which annealing graphene during imaging in standard vacuum reduces beam damage and beam-induced deposition of carbon.[196] Interactions between the beam and gases such as oxygen in the column are known from oxygen etching of graphene *in situ*[197,198] and from beam-induced deposition of silicon oxides on flowing disilane in an oxygen background.[199] UHV sample preparation may also minimize side reactions that complicate interpretation. For example, annealing graphene in vacuum prevents the reactions between deposited titanium, background gases, and adventitious C that lead to the unwanted formation of TiC.[200] Since analogous findings are likely to apply for other materials, UHV sample treatment and imaging conditions will greatly enhance experiments requiring quantitative spectroscopy.

In UHV-TEMs, such as the early VG microscopes and the Nion system discussed in **Section 3.4**, EELS is a key capability that is straightforwardly added. EDS appears less readily compatible with UHV-TEM. The EDS detector is located as close as possible to the sample; its components may be challenging to bake, and retraction mechanisms require re-engineering for UHV. To map changes in composition, future UHV-TEMs that include EELS and EFTEM will benefit from a direct electron detector to increase the readout speed.[201,202] Combining this with stable, low drift stages offer prospects for atomic resolution spectroscopy for *in situ* UHV-TEM experiments.[201]

5.3.3 Direct comparison of experiment and theory

While the microscopy community focuses on resolving smaller and smaller structures, down to single or few atoms, the computation community focuses on simulating the behavior of larger and larger structures via efficient algorithms and increased computing power. We are now entering a paradigm in which these two size regimes meet, allowing direct comparison of atomic scale observation with *ab-initio* or molecular dynamic simulations. Increased computational resources provide another benefit too: the fast and accurate simulation of TEM images via multislice simulation, with fast sweep (1-2 mins) simulations allowing rapid analysis of defocus and thickness values. Multiple open-source software packages are currently available.[203] High throughput materials computation can also be combined with experimental methods as discussed in **Section 5.2.2**. As these modeling techniques improve, detailed experiments in UHV environments provide ideal data for analysis, by minimizing extraneous impurities and side reactions that are not included in theoretical predictions. Close collaboration with the fields of data science and computational materials science presents a wealth of opportunities for *in situ* UHV-TEM.

5.4 Advances in instrumentation

5.4.1 In situ cartridge holders

Sample holders with a diverse range of functionalities such as electrical biasing, heating, cooling (even to liquid helium temperatures), closed gas cell, straining, and optical probes offer multiple prospects when combined with *in situ* UHV-TEM. Integration of functional sample holders with drift correction in UHV-TEM instruments will open opportunities for experiments that involve *in situ* stimuli while requiring a precisely controlled environment. We envisage complex experiments where, for example, growth is combined with a stimulus available from the sample holder: deposition on a substrate during straining, electromigration of single atoms deposited on clean surfaces during electrical biasing, optical response of individual catalytic particles or defects, phase transformations or effects of controlled deposition on quantum materials cooled below their transition temperature, or the influence of electric field on crystal growth. An enticing opportunity is to combine several capabilities in a holder, such as heating/cooling, biasing, straining and control of magnetic fields, and aim for high-throughput studies of material dynamics in controlled UHV conditions.

This broad range of external stimuli is already established in conventional microscopy[9,11] and advances in MEMS technology offer customized heating and biasing chips that are also compatible with UHV. However, for *in situ* UHV-TEM with integrated side chambers, a complication is that the sample is mounted on a cartridge such that it can be moved between UHV-TEM and other UHV preparation or characterization chambers. Direct feedthrough of

electrical or temperature connections from an external controller along the sample rod to the sample is therefore not possible. UHV-TEM cartridge holders instead use electrical connections in the microscope stage to couple to electrical feedthrough ports for heating and biasing. With suitable chips, these feedthroughs could also be utilized for *in situ* straining, excitation of on-chip LEDs or lasers, and Peltier cooling. Optical excitation sources can be integrated directly into ports in the column for light-coupled *in situ* reactions.[204,205]

Cryo-holders present additional challenges, but strategies are under development for flowing liquid N_2 and He to cool a cartridge-mounted sample, as well as for UHV transfer to connected chambers while maintaining cryogenic conditions. Side entry cryo-transfer holders and vacuum suitcases already allow transfer of samples between different UHV systems while maintaining cryogenic temperatures and vacuum conditions. It will be interesting to see the extent to which these may be adapted for ultra-high vacuum and compatibility with multiple chambers. Cryo-TEMs in the biological sciences currently employ autoloaders for sample cassettes, and it is possible that automated cryo-cartridge holders can be adapted for transfer between integrated UHV-TEMs and connected UHV systems for experiments that require it. We believe that the use of cooling holders in UHV-TEM represents a particularly exciting subset of the general opportunities discussed above, particularly for emerging quantum materials discussed further in **Section 5.5.3**.[206] However, for many dynamic crystal growth experiments, liquid nitrogen cooling may not be needed and it may be sufficient to focus on Peltier and intermediate cooling strategies. Therefore, it is important to consider the economic and informational trade-offs in each experimental set-up.

We have already mentioned closed gas cells as a strategy for executing higher pressure gas experiments, such as oxidation, corrosion, and reactive epitaxy. These are not readily bakeable for UHV, but a UHV-compatible design would allow for both higher pressure and more accurate determination of gas phase reactants and catalytic properties in UHV experiments, if the output gas flow is connected to a mass spectrometer. UHV closed cells would also allow UHV experiments to be carried out in conventional microscopes, making UHV studies more accessible without other specialized equipment. It is an engineering challenge to avoid incompatible materials such as porous ceramics or gaskets that outgas to the sample region, and long gas supply lines that are difficult to pump, but advances in materials design for bakeable UHV membranes, sealants, and gas lines may enable progress. However, closed cells still require viewing the sample through two membranes, so a closed cell experiment is not ideal for low dose and high resolution studies.

In the technological development of all holders (particularly variable temperature holders), a key practical aspect is drift correction or compensation mechanisms to allow continuous atomic resolution imaging during operation.[11,207] This is particularly important in envisioned future uses of *in situ* UHV-TEM where single atom diffusion and observation of molecular intermediates on surfaces is disrupted by even small amounts of drift. For denoising low dose *in situ* UHV-TEM data, sample stability is just as critical. Moreover, freeing the operator from having to track and reset the sample position enables attention to be directed to optimizing other important experimental variables.

5.4.2 Column and sample area modifications

Beyond specialized *in situ* holders, innovations in the microscope column design represent a more ambitious task, but one with the potential for a dramatic expansion in the types of experiments that can be envisioned.

Aberration correction and monochromation enable atomic resolution imaging at low accelerating voltages, which will benefit *in situ* UHV-TEM studies involving beam-sensitive materials. Good imaging performance has been demonstrated in (non-UHV) instruments designed for operation at voltages as low as 15-20 keV.[208,209] Chromatic aberration (C_c) generally limits resolution at low voltage; its correction is complex and expensive (compared to C_s correction) but is worthwhile in specific applications.[210–212] Widening the pole-piece gap is another design choice for the column, offering a larger sample area for integrating *in situ* capabilities such as deposition sources or lasers via ports in the pole piece or column, additional detectors (e.g. SEM or Auger), transport measurement probes, and stable low temperature stages and cryostats.[15,213] This comes at the cost of resolution, but with aberration correction to improve performance, could realize the promise of fully integrated *in situ* systems such as SHEBA, as discussed in **Section 3.4**. Widening the pole piece gap has already had major effects in the emerging technique of atomic electron tomography (AET), where 3D reconstruction of nanoparticles is achieved through imaging at a series of sample tilts.[214] In one recent (non-UHV) example, a secondary electron detector installed in the widened pole piece enabled placement of electrical probes on pre-defined contact pads, and an electrostatic biprism enabled mapping of electric and magnetic fields.[213]

Reducing the sample holder volume is an alternative approach that avoids the resolution penalty of widening the gap. Microfabrication can produce small samples with heating or other functionalities that allow for smaller volume holders or cartridges and, hence, higher tilt angles. This may particularly help in UHV-TEM studies of dynamic crystal growth, where both plan view and tilted view of surfaces and interfaces are useful. Moreover, on-chip logic could be utilized for integrated LED lasers, circuits, and other capabilities. Whether using a widened pole piece gap or miniaturized samples, care must be taken to ensure all materials are UHV compatible.

With such advances, we can imagine increasingly complex *in situ* capabilities. Integration of optical fibers for photon irradiation or on-chip LEDs can be combined with UHV-TEM to study photocatalysis and phase transitions of low-dimensional nanostructures. UHV-TEM is particularly useful here since catalytic reaction pathways are determined by surface adsorbates, as discussed further in **Section 5.5**. Laser integration can also generate Raman and pump-probe signals. The integration of spectroscopic techniques puts the potential of full structural, chemical, and optical characterization on the horizon.[215,216] Separately, cryo-holders cooled by liquid helium can practically reach temperatures around 6-20 K, with lower temperature operation partially limited by radiation losses and poor heat shielding from the nearby objective lenses. A large investment would be required to bring standard cryo technology into the limited space around the sample, with challenges in minimizing vibrations due to coolant flow and evaporation. Redesigning the sample area could push the sample temperature to below 1 K in specialized microscopes to observe growth phenomena and structural, magnetic and electronic phase transformations under controlled environment. Finally, even more ambitious designs involving C_s/C_c correction envisage a large enough polepiece gap to accommodate both electron microscopy and synchrotron radiation beam lines.[212] AET and correlative synchrotron experiments could both be of interest when the sample environment is UHV and deposition or other materials modification capabilities are available *in situ*.

5.4.3 Increased temporal resolution

We have described phenomena in this review that generally occur in the second or millisecond time range. However, key phenomena such as sub-critical fluctuations, diffusion, and interfacial transport occur within microseconds of flux activation, while atomic adsorption, electronic excitations, and phonon dynamics may occur in the nano- or even pico-second regime. Conventional TEM is limited to hundreds or thousands of frames per second by the read-out frequency of the camera, the beam current, which determines the signal to noise ratio of each frame, and the dose rate and total dose that can be tolerated by the sample. As mentioned in **Section 5.2.3**, advanced electron detection provides a benefit to temporal resolution due to its ability to measure the time and position of each individual electron detection event.[185]

As well as detector development, other methods extend the temporal resolution of *in situ* TEM.[217,218] One of these is the use of pulsed electron sources controlled by optical[37] or electronic[219] means, capable of reaching ~10 GHz pulses. These methods are generally limited to imaging repeatable processes by pump-probe techniques and are less suitable for nucleation and diffusion studies. Development of a 'single shot' approach, which generates short pulses with enough electrons to form images, allows sequential capturing of processes, and has achieved a temporal resolution ~15 nanoseconds[220] and spatial resolution < 5 nm.[11] Such systems can be limited by Coulomb interactions, and require redesign of the electron optics.[221] Experiments that may justify this additional investment in complexity include irreversible growth events such as diffusion, nucleation, growth dynamics, and dynamics of small atomic clusters at the femtosecond scale.[222,223]

5.4.4 Fully integrated UHV fabrication and characterization systems

As conventional electron microscopy continues its evolution from a means of acquiring static images to a broad range of 'experimental laboratories' inside the polepiece, we anticipate a similar trend of increasing experimental complexity for the UHV experiments performed directly in the column or in connected side chambers. This involves incorporating capabilities such as surface science probes (AES, XPS, LEED), sample preparation, ion beam irradiation, optical spectroscopy, cathodoluminescence, photoluminescence, gas chromatography, magnetic measurements, and abilities to observe 3D structure (tomography) and to apply electrochemical or opto-electronic stimuli. Since not all these tools will be in the polepiece, sample transfer while maintaining UHV environment is essential in these systems. Maintaining sample temperature while transferring is a more difficult design task but would create additional functionalities. More expansive side chambers could be imagined to incorporate systems such as synchrotron-TEM correlative imaging, x-ray diffraction, gloveboxes, APT, STM, low temperature optical spectroscopy, and ARPES. The addition of side chambers can result in transmission of vibrations, and while some experiments will benefit largely from the additional complexity, others may be more suited to vacuum transfer suitcases.

One of the most striking examples of the potential of 'lab in a microscope' integration is the measurement, in 1999, of quantized conductance in Au nanobridges. Using a niche combination of an *in situ* TEM and STM UHV microscope, Takayanagi *et al.* obtained atomic resolution images and simultaneous conductance measurements of rows of Au atoms during *in situ* straining.[224] This verified the conductance of a single strand of atoms to be quantized as $G_0=2e^2/h$, and showed that equipartition holds true for quantum systems. This remains a remarkable experimental observation today, over 20 years later, and begs the question: with our current technological advancements, what observations could we imagine in the next 20

years inside the well-controlled environment of a UHV electron microscope? In the final sections we speculate on some possibilities.

5.5 Perspectives on key scientific questions

In the DOE Report on Basic Research Needs for Transformative Experimental Tools,[225] the highest-level conclusions include the following: "...the quest for deeper scientific insights and the drive to control chemistry and materials at the atomic and molecular levels require increasingly powerful and sophisticated instruments." The ability of *in situ* UHV-TEM to provide unique information about dynamic crystal growth phenomena is applicable to a variety of emerging materials classes, especially if we assume some success in the developments described in **Section 5.4**. **Figure 10** illustrates some fundamental details of nucleation and growth processes that future *in situ* UHV-TEM would be uniquely poised to uncover. At the smallest length scale are adsorption and surface reactions of individual atoms from the gas phase, which could bring transformative insights for catalysis studies. Over longer dimensions, atomic motion along the surface and sub-critical fluctuations including bond breaking and diffusion could be analyzed. Once critical nuclei have formed, the initial stages of growth and properties of atomic clusters can be determined. And at even larger length scales, the formation and characterization of defects and interfaces can be addressed. Low dose and low electron energy imaging increase the possibilities of TEM to study the beam-sensitive materials prevalent in physics and technology today, including 2D material heterostructures, metal organic frameworks, biomaterials, and single defect states. In combination with the controlled environment of UHV and additional specialized imaging modes, this unlocks a variety of opportunities across quantum materials, energy materials, electronic and photonic materials, and materials in extreme environments.

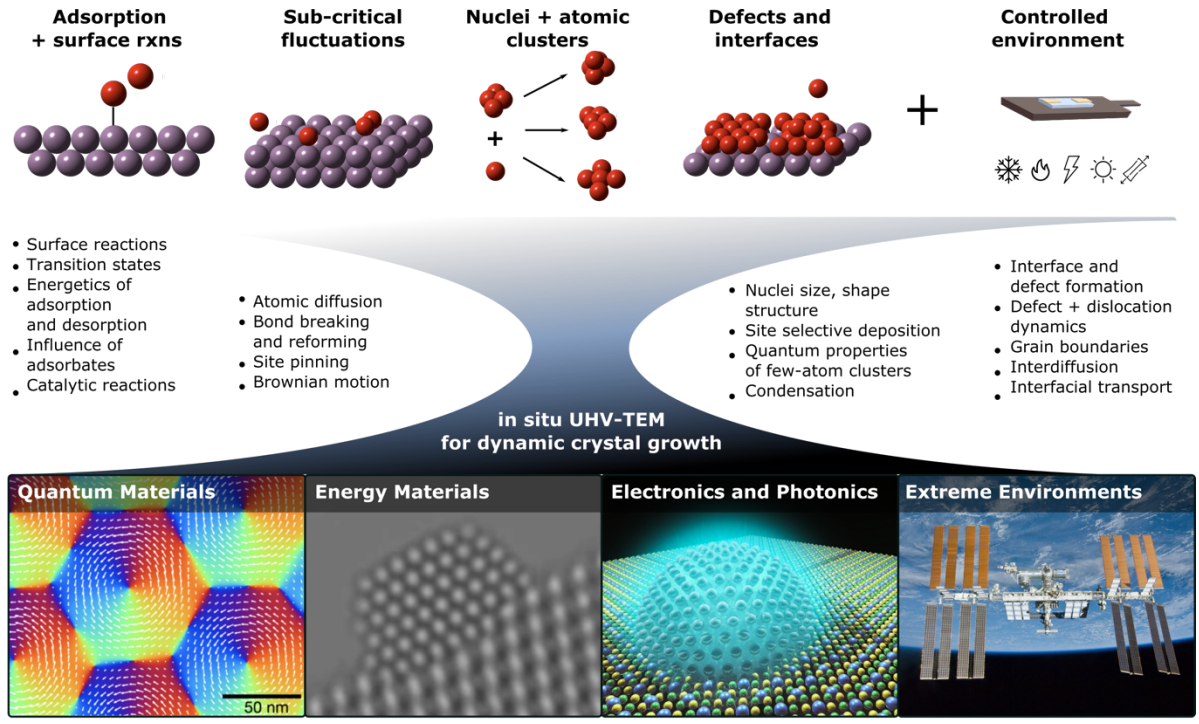

Figure 10: Schematic of dynamic crystal growth phenomena that can be studied with *in situ* UHV-TEM with current technical advances at different length scales, from individual atomic adsorption to the formation of grain boundaries, thin films, and interfaces. Below shows overview of example research fields that could be impacted: (1) quantum materials (image from [226]), (2) energy materials (image from [227]) (3) electronic and photonic materials (image

credit: Sean Kelley (https://inform.studio)), (4) materials in extreme environments, e.g. space among others (image credit: NASA).

5.5.1 Quantum materials

Growth and characterization of quantum materials - defined as solids with exotic physical properties arising from the collective quantum mechanical properties of their constituent electrons[228,229] – present a significant future growth area for UHV-TEM. Proposed as the building blocks of next-generation information technology, quantum materials nevertheless exhibit ubiquitous disorder[230,231] which significantly affects their properties. This makes fabrication of novel devices challenging, particularly those that require nanoscale dimensions, where adsorbates, disorder, interfaces, and finite-size effects govern materials properties. TEM is an essential tool because it can probe the degrees of freedom that determine quantum material properties (lattice, spin, charge, and orbital): the structure can be imaged with atomic resolution, spin textures and charge distributions can be mapped by Lorentz TEM, holography, and DPC, and orbital occupancy can be probed with EELS.[183,229,232,233]

In situ UHV-TEM methods for growth and simultaneous characterization of quantum materials at the atomic scale will build on such measurements. One could study and control the nucleation and growth of superconductors and other easily-oxidizable materials that require UHV conditions, making use of equipment where deposition chambers such as MBE are connected to the UHV-TEM. The role of oxides, adsorbates, and contaminants on quantum decoherence and other properties could be probed within the pristine UHV environment. Topological surface states and charge density wave pinning at defects, interfaces, and small atomic clusters could be studied by combining *in situ* UHV-TEM imaging with DPC or diffraction. Similarly, the influence of individual magnetic atoms or clusters on magnetic domains, or spin-orbit coupling via metal deposition on magnetic thin films can be studied. The critical temperature of magnetic and superconducting transitions is also known to vary with increasing thickness of material, which could be studied via *in situ* layer-by-layer deposition in UHV. Moreover, in quantum structures formed by stacking 2D van der Waals materials[234], individual vacancy defects can function as single photon emitters in transition metal dichalcogenides and hexagonal boron nitride. These defects are known to be air sensitive: encapsulation with boron nitride or graphene limits degradation and decreases line-width of EELS spectra.[235–237] Device fabrication requires understanding and control of the creation, removal, and processing of such defects, including their reactions with oxygen or dopant species, in which UHV excels. Integrated UHV-TEM experiments to study such phenomena could involve a glove box connected to the UHV-TEM system for fabrication of heterostructures of air-sensitive 2D materials.

Correlated physical phenomena in quantum and magnetic materials, for example magnetic transitions, many-body excitations, defect emission and superconductivity, often emerge at low temperature.[206] UHV conditions are standard in low temperature physics to reduce contamination effects. Low temperatures also reduce the damage rate of many materials in TEM.[233,238] We therefore anticipate that UHV-TEM imaging with cryogenic sample transfer and magnetic/optical measurements in connected chambers could elucidate the origins of many of these phenomena.

5.5.2 Energy materials

The controlled environment and *in situ* capabilities of UHV-TEM provide a powerful platform for studying energy materials. One of the most promising is the direct imaging of catalytic reaction pathways.[239] Many catalytic reactions critical for energy materials would benefit from such insights, including water splitting, CO_2 reduction, hydrocarbon cracking, and oxygen evolution. Catalytic processes involve the formation of transition states, in which short-lived intermediate species exist temporarily on the catalyst surface. *In situ* UHV-TEM, combined with advanced denoising procedures, could help elucidate the transition states and reaction pathways under well-controlled conditions, producing information to optimize catalyst efficiency. The UHV environment, although different from realistic reaction conditions, may even facilitate the direct observation of light element molecules such as H_2, CO, CH_4, and O_2 adsorbed on catalytic nanoparticle surfaces, where weak contrast among impurity adsorbates[240,241] poses challenges for conventional ETEM. The cyclic nature of catalytic reactions offers intriguing possibilities for improving signal-to-noise by averaging signals from the same metastable state.[239] External triggers, such as light or electric field pulses, can be used to make the turnover process periodic and allow for more controlled experimentation and data analysis.[239]

Atomic level understanding of transport processes, such as electron and ion transport, is also necessary for optimizing energy materials design.[239] Ionic transport through ceramics is particularly important in electrochemical technologies, and understanding the influence of individual defects, adsorbates, and surface treatments in UHV would be beneficial. Point defects in these materials bind impurity adsorbates when not in UHV conditions, leading to local changes in transport, bonding, and lattice distortion. Other interesting questions in energy materials include the role of defects and impurities in the performance of photovoltaic materials, examined without interference from ambient gases; the nucleation and behavior of nanoparticles with well-controlled surfaces in photocatalytic materials; atomic-scale structure and dynamics of perovskite solar cells that are particularly air-sensitive; and investigating atomic-scale mechanisms of corrosion in energy-related materials. For extremely air-sensitive electrochemical materials, *in situ* UHV-TEM coupled with a glove box or other fabrication chamber would provide benefits, and the ultra-clean environment of UHV would allow close comparison with modeling without extraneous impurities. Specialized imaging modes could allow determination of individual chemical species and adsorbates (even with isotopic sensitivity[242]), and the additional ability to control temperature, light intensity, bias, and apply other processing in integrated UHV systems would allow for the examination of how these variables affect real-world performance.

5.5.3 Electronic and photonic materials

UHV-TEM provides unique information regarding materials for emerging electrical and photonic devices, such as semiconductors, quantum dots, nanowires, and 2D heterostructures. In particular, the UHV environment is essential for growth and surface reactions in semiconductors such as silicon, which oxidize readily in poorer TEM vacuums. Opportunities for dynamic *in situ* UHV-TEM include observing the adsorption and reaction of individual atoms on the surface of air-sensitive materials (silicon, 2D magnets, perovskites), analyzing atomic motion and diffusion at the surface and within materials like silicon or gallium nitride, characterizing the initial stage of growth and properties of 2D heterostructures and metal-organic frameworks, investigating the properties of single defect states in a variety of opto-electronic materials, determining the influence of epitaxy on charge transfer across interfaces,[243,244] and examining the influence of growth conditions on quantum dots, nanowires, and other self-assembled structures relevant to opto-electronic devices. Adding optical

spectroscopy methods to the UHV-TEM column would be particularly beneficial for opto-electronic materials. Through UHV experiments, it will become possible to gain a detailed understanding of the fundamental processes that govern the growth and characterization of these materials and how they may be optimized for use in devices.

Important developing techniques for *in situ* nanoscale manufacturing of electronic and photonic devices include area-selective deposition, interface control, templated growth, and heterostructure formation. Here, possibilities emerge to fully fabricate and even contact devices within the TEM column or in side chambers. In combination with the automation and side chamber facilities described in **Sections 5.2.1 and 5.4.4,** we may eventually envision a device fabrication and characterization pipeline, analogous to what is currently implemented for semiconductor wafer failure analysis, but entirely carried out at the atomic scale and in controlled vacuum.

5.5.4 Expanding horizons for UHV-TEM

An unexpected benefit of the UHV environment is that it can be used to replicate exotic conditions found in space or other atmospheres. For example, astrophysicists have used a liquid He cooling holder combined with *in situ* gas injection in UHV-TEM to observe the nucleation and growth of CO and CO_2 crystals on amorphous solid water at 10 K.[245] The activation energies obtained from these studies clarify surface reaction mechanisms in the initial stages of the evolution of molecular clouds.[245] Radiation-hard materials can be studied by generating defects with various radiation sources incorporated in UHV side chambers and imaging these defects without atmospheric exposure.

These are examples where the reach of UHV-TEM for growth phenomena is already extending to fields beyond materials science. We anticipate further opportunities, given the fundamental importance of nucleation and growth mechanisms over a wide range of scientific and technological fields in chemistry, biology, physics and beyond. We suggest that UHV-TEM will play a particularly critical role at low temperature. Here, many phenomena await discovery involving growth and phase transformations. For example, low temperature non UHV-TEM growth experiments have already probed the condensation of water on controlled surfaces;[246] self-assembled monolayer formation;[247] and the formation of noble gas crystals and condensates.[248,249]

Different types of defects (e.g., vacancies, dislocations, moiré reconstructions) will affect nucleation and growth of materials in distinct ways to tailor site-selective deposition in UHV. Similarly, surface reconstructions and terraces influence the growth of thin films, enabling the development of thin film technologies with improved performance and reliability. UHV-TEM will help us understand how impurities, contaminants, and surface terminations (e.g. O_2, H_2) affect the initial stages of nanocrystal formation; how different growth conditions (temperature, pressure, strain, electric field) influence the atomic-scale structure, composition, and properties of nanocrystals; and how substrate materials and orientations influence newly-discovered complex epitaxial growth modes (e.g. chiral epitaxy, phase selection, and van der Waals) and properties of the resulting materials. Moreover, direct visualization of these growth processes will allow comparison with modeling to extract fundamental physical constants such as adsorption energies, interaction energies, surface diffusion constants, interface energies, interdiffusion, dewetting behavior, sintering, and reaction energies for direct comparison with theory. Answering these scientific questions will not only further our fundamental

understanding of nucleation and growth, but also have practical implications for a wide range of scientific and technological fields.

Acknowledgements
K.R. acknowledges funding and support from a MIT MathWorks Engineering Fellowship and ExxonMobil Research and Engineering Company through the MIT Energy Initiative. J.D.T. acknowledges support from Independent Research Fund Denmark though Grant Number 9035-00006B. The authors would like to acknowledge anonymous reviewers for helpful feedback, Paul Miller, Dr. Julian Klein, and Prof. Juan Carlos Idrobo for useful discussions on future perspectives, Prof. David Muller, Prof. Judith Yang, and Dr. Arno Bleeker for useful historical microscope information, and Dr. George Varnavides for graphical support.

References

1. Kuech, T. & Nishinaga, T. *Handbook of Crystal Growth*. *Second Ed.* (Elsevier, 2014). doi:10.1016/b978-0-444-88908-9.50001-2

2. Pimpinelli, A. & Villain, J. *Physics of Crystal Growth*. (Cambridge University Press, 1998). doi:10.1017/cbo9780511622526

3. Venables, J. A. Atomic processes in crystal growth. *Surf. Sci.* **299–300,** 798–817 (1994).

4. Poppa, H. High resolution, high speed ultrahigh vacuum microscopy. *JVSTA* **22,** 1931 (2004).

5. Smith, D. J., Gajdardziska-Josifovska, M., Lu, P., McCartney, M., Podbrdsky, J., Swarm, P. & Jones, J. Development and applications of a 300 keV ultrahigh-vacuum high-resolution electron microscope. *Ultramicroscopy* **49,** 26–36 (1993).

6. Chiaramonti, A. N. & Marks, L. D. Atomic Resolution Transmission Electron Microscopy of Surfaces. *J. Mater. Res.* **20,** 1619–1627 (2005).

7. Marks, L. D. Experimental studies of small particle structures. *Reports Prog. Phys.* **57,** 603–649 (1994).

8. Yagi, K., Kobayashi, K., Tanishiro, Y. & Takayanagi, K. In situ electron microscope study of the initial stage of metal growth on metals. *Thin Solid Films* **126,** 95–105 (1985).

9. Ross, F. M. & Minor, A. M. *In situ transmission electron microscopy*. *Springer Handbooks* (Springer, 2019). doi:10.1007/978-3-030-00069-1_3

10. Pienack, N., Bensch, W., Bensch, W. & Pienack, N. In-Situ Monitoring of the Formation of Crystalline Solids. *Angew. Chemie Int. Ed.* **50,** 2014–2034 (2011).

11. Taheri, M. L., Stach, E. A., Arslan, I., Crozier, P. A. A., Kabius, B. C., Lagrange, T., Minor, A. M., Takeda, S., Tanase, M., Wagner, J. B. & Sharma, R. Current status and future directions for in situ transmission electron microscopy. *Ultramicroscopy* **170,** 86–95 (2016).

12. Zheng, H., Meng, Y. S. & Zhu, Y. Frontiers of in situ electron microscopy. *MRS Bull.* **40,** 12–18 (2015).

13. De Yoreo, J. J. & Sommerdijk, N. A. J. M. Investigating materials formation with liquid-phase and cryogenic TEM. *Nat. Rev. Mater.* **1,** 1–18 (2016).

14. Batson, P. E., Dellby, N. & Krivanek, O. L. Sub-aångstrom resolution using aberration corrected electron optics. *Nature* **418,** 617–620 (2002).

15. Krivanek, O. L., Corbin, G. J., Dellby, N., Elston, B. F., Keyse, R. J., Murfitt, M. F., Own, C. S., Szilagyi, Z. S. & Woodruff, J. W. An electron microscope for the aberration-corrected era. *Ultramicroscopy* **108,** 179–195 (2008).

16. Krivanek, O. L., Chisholm, M. F., Nicolosi, V., Pennycook, T. J., Corbin, G. J., Dellby, N., Murfitt, M. F., Own, C. S., Szilagyi, Z. S., Oxley, M. P., Pantelides, S. T. & Pennycook, S. J. Atom-by-atom structural and chemical analysis by annular dark-field electron microscopy. *Nature* **464,** 571–574

(2010).

17. Haider, M., Uhlemann, S., Schwan, E., Rose, G., Kabius, B. & Urban, K. Electron microscopy image enhanced. *Nature* **392,** 768–769 (1998).

18. Poppa, H. Advanced experimental approach to model studies of supported metal particle systems. *Top. Catal.* **13,** 139–146 (2000).

19. Jayaram, G., Plass, R. & Marks, L. D. UHV-HREM and diffraction of surfaces. *Interface Sci.* **2,** 379–395 (1995).

20. Cowley, J. M. Applications of STEM instruments for surface studies. *Surf. Rev. Lett.* **4,** 567–575 (1997).

21. Marks, L. D., Ai, R., Bonevich, J. E., Buckett, M. I., Dunn, D., Zhang, J. P., Jacoby, M. & Stair, P. C. UHV microscopy of surfaces. *Ultramicroscopy* **37,** 90–102 (1991).

22. Robinson, A. L. Consensus on silicon surface structure near. *Science.* **232,** 451–453 (1986).

23. D. P. Woodruff. *Modern Techniques of Surface Science*. (Cambridge University Press, 2016).

24. Hansma, P. K. & Tersoff, J. Scanning tunneling microscopy. *J. Appl. Phys.* **61,** R1 (1998).

25. Patel, D. I., Roychowdhury, T., Jain, V., Shah, D., Avval, T. G., Chatterjee, S., Bahr, S., Dietrich, P., Meyer, M., Thißen, A. & Linford, M. R. Introduction to near-ambient pressure x-ray photoelectron spectroscopy characterization of various materials. *Surf. Sci. Spectra* **26,** 016801 (2019).

26. Marks, L. D., Xu, P. & Dunn, D. N. UHV transmission electron microscopy of Ir(001): II. Atomic positions of the (5 × 1) reconstructed surface from HREM and R-factor refinements. *Surf. Sci.* **294,** 322–332 (1993).

27. Dunn, D. N., Xu, P. & Marks, L. D. UHV transmission electron microscopy of Ir(001): I. Microstructure of the (1 × 1) and the reconstructed (5 × 1) surfaces. *Surf. Sci.* **294,** 308–321 (1993).

28. Takeguchi, M., Wu, Y., Tanaka, M. & Furuya, K. In situ UHV-TEM observation of the direct formation of $PdSi_2$ islands on Si 111 surfaces at high temperature. *Appl. Surf. Sci.* **159,** 159–160 (2000).

29. Twesten, R. D., Gibson, J. M. & Ross, F. M. Visualization of Dynamic Near-Surface Processes. *MRS Bull.* **19,** 38–43 (1994).

30. Zhou, G. & Yang, J. C. In situ UHV-TEM investigation of the kinetics of initial stages of oxidation on the roughened Cu(1 1 0) surface. *Surf. Sci.* **559,** 100–110 (2004).

31. Anton, R. & Schneidereit, I. In situ TEM investigations of dendritic growth of Au particles on HOPG. *Phys. Rev. B* **58,** 20 (1998).

32. Petroff, P. M., Chen, C. H. & Werder, D. J. Microscopy of surfaces and applications to molecular beam epitaxy. *Ultramicroscopy* **17,** 185–191 (1985).

33. Ritley, K. A. & Flynn, C. P. Growth of b-axis rare earths on sapphire by molecular beam epitaxy. *Appl. Phys. Lett.* **72,** 170–172 (1998).

34. Venables, J. A., Smith, D. J. & Cowley, J. M. HREM, STEM, REM, SEM — and STM. *Surf. Sci.* **181,** 235–249 (1987).

35. Collazo-Davila, C., Landree, E., Grozea, D., Jayaram, G., Plass, R., Stair, P. & Marks, L. D. Design and Initial Performance of an Ultrahigh Vacuum Sample Preparation Evaluation Anlaysis and Reaction (SPEAR) System. *JMSA* **1,** 267–279 (1995).

36. Venables, J. A., Hembree, G. G., Drucker, J., Crozier, P. A. & Scheinfein, M. R. The MIDAS project at ASU: John Cowley's vision and practical results. *J. Electron Microsc.* **54,** 151–162 (2005).

37. Zewail, A. H. 4D ultrafast electron diffraction, crystallography, and microscopy. *Annu. Rev. Phys. Chem.* **57,** 65–103 (2006).

38. Sharma, R. An environmental transmission electron microscope for in situ synthesis and characterization of nanomaterials. *J. Mater. Res.* **20,** 1695–1707 (2005).

39. Zheng, H. & Zhu, Y. Perspectives on in situ electron microscopy. *Ultramicroscopy* **000,** 1–9 (2017).

40. Phatak, C., Petford-Long, A. K. & De Graef, M. Recent advances in Lorentz microscopy. *Curr. Opin. Solid State Mater. Sci.* **20,** 107–114 (2016).

41. Butler, E. & Hale, K. *Dynamic experiments in the electron microscope*. (North-Holland Pub. Co., 1981).

42. In Situ TEM Holders & Sample Supports | Protochips. *Accessed: 2022-12-26* at <https://www.protochips.com/products/>

43. Direct Electron – Innovation Propelling Discovery. *Accessed: 2022-12-26* at <https://www.directelectron.com/>

44. Bassett, G. ., Menter, J. . & Pashley, D. . Moiré patterns on electron micrographs, and their application to the study of dislocations in metals. *Proc. R. Soc. London.* **246,** 345–368 (1958).

45. Pashley, D. W., Menter, J. W. & Bassett, G. A. Observation of dislocations in metals by means of moiré patterns on electron micrographs. *Nature* **179,** 752–755 (1957).

46. Pashley, D. W., Stowell, M. J., Jacobs, M. H. & Law, T. J. The growth and structure of gold and silver deposits formed by evaporation inside an electron microscope. *Philos. Mag.* **10,** 127–158 (1964).

47. McLauchlan, T. A., Sennett, R. S. & Scott, G. D. Continuous Observations With the Electron Microscope on the Formation of Evaporated Films of Silver, Gold, and Tin. *Can. J. Res.* **28a,** 530–534 (1950).

48. Poppa, H. Heterogeneous Nucleation of Bi and Ag on Amorphous Substrates (In Situ Electron Microscopy Studies). *J. Appl. Phys.* **38,** 3883 (1967).

49. Ruska E. The early development of electron lenses and electron microscopy. *Microsc Acta Suppl.* **5,** 1–140 (1980).

50. Bassett, G. A. Continuous observation of the growth of vacuum evaporated metal films. *Proceeding Eur. Reg. Conf. Electron Microsc.* **5,** 709–716 (1960).

51. Stowell, M. J. & Law, T. J. The growth and defect structure of gold films formed on molybdenite in ultra-high vacuum. *Phys. Status Solidi* **25,** 139–146 (1968).

52. Yoshimura, N. *Historical evolution toward achieving ultrahigh vacuum in JEOL electron microscopes*. *SpringerBriefs Appl. Sci. Technol.* (Springer Verlag, 2014).

53. Wardell, I. R. M. & Bovey, P. E. Chapter 6 A History of Vacuum Generators' 100-kV Scanning Transmission Electron Microscope. *Adv. Imaging Electron Phys.* **159,** 221–285 (2009).

54. Valdrè, U., Robinson, E. A., Pashley, D. W., Stowell, M. J. & Law, T. J. An ultra-high vacuum electron microscope specimen chamber for vapour deposition studies. *J. Phys. E.* **3,** 501–506 (1970).

55. Takayanagi, K., Yagi, K., Kobayashi, K. & Honjo, G. Techniques for routine UHV in situ electron microscopy of growth processes of epitaxial thin films. *J. Phys. E.* **11,** 441–448 (1978).

56. Honjo, G., Takayanagi, K., Kobayashi, K. & Yagi, K. Ultra-high vacuum in sity electron microscopy of growth processes of epitaxial thin films. *J. Cryst. Growth* **42,** 98–109 (1977).

57. Heinemann, K. & Poppa, H. An ultrahigh vacuum multipurpose specimen chamber with sample introduction system for in situ transmission electron microscopy investigations. *J. Vac. Sci. Technol. A* **4,** 127 (1986).

58. Moorhead, R. D. & Poppa, H. -. in *Proc. 27th EMSA Meet.* 116 (Claitors, 1969).

59. Xu, P., Miller, P. & Silcox, J. The nucleation and epitaxial growth of Au and Ag on thin silicon studied

with a scanning transmission electron microscope. *MRS Online Proc. Libr.* **202,** 19–24 (1990).

60. McDonald, M. L., Gibson, J. M. & Unterwald, F. C. Design of an ultrahigh-vacuum specimen environment for high-resolution transmission electron microscopy. *Rev. Sci. Instrum.* **60,** 700 (1989).

61. McDonald, M. L. & Gibson, J. M. An ultrahigh vacuum and ultrahigh resolution transmission electron microscope. in *Proc. 42nd EMSA* (ed. Bailey, G. W.) 436–437 (San Francisco Press, 1984).

62. Marks, L. D., Kubozoe, M., Tomita, M., Ukiana, M., Furutse, T. & Matsui, I. Design and initial performance of a UHV-HREM. in *Proc. 46th EMSA* (ed. Bailey, G. W.) 658–659 (San Francisco Press, 1988).

63. Yata, M., Toda, A., Nagatsuyu, H., Hariu, T., Nakada, T., Tsukui, K. & Osaka, T. Ultrahigh vacuum in situ transmission electron microscopy observations of molecular-beam epitaxially grown InSb(111). *J. Appl. Phys.* **63,** 5751 (1988).

64. Metois, J. J., Nitsche, S. & Heyraud, J. C. An ultra-high vacuum transmission and scanning electron microscope for crystal growth experiments. *Ultramicroscopy* **27,** 349–358 (1989).

65. Hembree, G. G., Crozier, P. A., Drucker, J. S., Krishnamurthy, M., Venables, J. A. & Cowley, J. M. Biassed secondary electron imaging in a UHV-STEM. *Ultramicroscopy* **31,** 111–115 (1989).

66. Wardell, I. R. M. Some design considerations concerning a STEM probe forming system. *Ultramicroscopy* **7,** 39–44 (1981).

67. Smith, D. J., Podbrdsky, J., Swann, P. R. & Jones, J. S. Initial Experiences with a 300-kV HREM Converted for UHV Operation. *MRS Online Proc. Libr.* **139,** 289 (1989).

68. Swann, P. R., Jones, J. S., Krivanek, O. L., Smith, D. J., Venables, J. A. & Cowley, J. M. -. in *Proc. 45th Annu. Meet. EMSA* 136 (1987).

69. Bleeker, A. J., Pijper, F. J. & Kruit, P. An ultra-high-vacuum chamber for a Philips EM430 stem. *Ultramicroscopy* **31,** 458–459 (1989).

70. Kondo, Y., Ohi, K., Ishibashi, Y., Hirano, H., Harada, Y., Takayanagi, K., Tanishiro, Y., Kobayashi, K. & Yagi, K. Design and development of an ultrahigh vacuum high-resolution transmission electron microscope. *Ultramicroscopy* **35,** 111–118 (1991).

71. Takayanagi, K., Tanishiro, Y., Kobayashi, K., Yamamoto, N., Yagi, K., Ohi, K., Kondo, Y., Hirano, H., Ishibashi, Y., Kobayahi, H. & Harada, Y. -. in *Proc. 11th Int. Congr. Electron Microsc.* (eds. Imura, T., Maruse, S. & T., S.) 1337 (Jpn. Soc. Of Electron Microscopy, 1986).

72. LeGoues, F. K., Reuter, M. C., Tersoff, J., Hammar, M. & Tromp, R. M. Cyclic growth of strain-relaxed islands. *Phys. Rev. Lett.* **73,** 300–303 (1994).

73. Anton, R., Reetz, O. & Schrnldt, A. A. Performance of turbomolecular pumps in an extended TEM specimen chamber equipped for in-situ vapour deposition experiments. *Ultramlcroscopy* **41,** 303–316 (1992).

74. Marshall, M. T., Mcdonald, M. L., Tong, X., Yeadon, M. & Gibson, J. M. A new surface science in situ transmission and reflection electron microscope. *Rev. Sci. Instrum.* **69,** 440 (1998).

75. Tanaka, M., Furuya, K., Takeguchi, M. & Honda, T. Surface observation of Mo nanocrystals deposited on Si (111) thin films by a newly developed ultrahigh vacuum field-emission transmission electron microscope. *Thin Solid Films* **319,** 110–114 (1998).

76. Sun, H. P., Chen, Y. B., Pan, X. Q., Chi, D. Z., Nath, R. & Foo, Y. L. Formation and evolution of epitaxial Co_5Ge_7 film on Ge (001) surface by solid-state reaction in an in situ ultrahigh-vacuum transmission electron microscope. *Appl. Phys. Lett* **87,** 211909 (2005).

77. Kouchi, A., Hama, T., Kimura, Y., Hidaka, H., Escribano, R. & Watanabe, N. Matrix sublimation method for the formation of high-density amorphous ice. *Chem. Phys. Lett.* **658,** 287–292 (2016).

78. Mangler, C., Meyer, J., Mittelberger, A., Mustonen, K., Susi, T. & Kotakoski, J. A Materials Scientist's CANVAS: A System for Controlled Alteration of Nanomaterials in Vacuum Down to the Atomic Scale. *Microsc. Microanal.* **28,** 2940–2942 (2022).

79. Elibol, K., Mangler, C., Gupta, T., Zagler, G., Eder, D., Meyer, J. C., Kotakoski, J. & Bayer, B. C. Process Pathway Controlled Evolution of Phase and Van-der-Waals Epitaxy in In/In_2O_3 on Graphene Heterostructures. *Adv. Funct. Mater.* **30,** 2003300 (2020).

80. Smith, D. J., Gajdardziska-Josifovska, M., Lu, P., McCartney, M. R., Podbrdsky, J., Swann, P. R. & Jones, J. S. Development and applications of a 300 keV ultrahigh-vacuum high-resolution electron microscope. *Ultramicroscopy* **49,** 26–36 (1993).

81. Kruit, P. Nanometer resolution analysis of surfaces. *Surf. Sci.* **287–288,** 1067–1069 (1993).

82. Hannon, J. B., Kodambaka, S., Ross, F. M. & Tromp, R. M. The influence of the surface migration of gold on the growth of silicon nanowires. *Nature* **440,** 69–71 (2006).

83. Kouchi, A., Furuya, K., Hama, T., Chigai, T., Kozasa, T. & Watanabe, N. Direct Measurements of Activation Energies for Surface Diffusion of CO and CO_2 on Amorphous Solid Water Using In Situ Transmission Electron Microscopy. *Astrophys. J. Lett.* **891,** L22 (2020).

84. Kizuka, T. & Tanaka, N. Atomistic visualization of epitaxial growth process using a new TEM specimen holder for vacuum-deposition. *Surf. Sci.* **386,** 249–253 (1997).

85. Yeadon, M., Yang, J. C., Averback, R. S. & Gibson, J. M. Sintering and oxidation using a novel ultrahigh vacuum transmission electron microscope with in situ magnetron sputtering. *Microsc. Res. Tech.* **42,** 302–308 (1998).

86. Gibson, J. M., Batstone, J. L. & Tung, R. T. In situ study of the molecular beam epitaxy of $CoSi_2$ on (111) Si by transmission electron microscopy and diffraction. *Appl. Phys. Lett* **51,** 45 (1987).

87. Bennett, P. A., Smith, D. J., He, Z., Reuter, M. C., Ellis, A. W. & Ross, F. M. In situ observations of endotaxial growth of $CoSi_2$ nanowires on Si(110) using ultrahigh vacuum transmission electron microscopy. *Nanotechnology* **22,** 305606 (2011).

88. Dai, S., Gao, W., Zhang, S., Graham, G. W. & Pan, X. Transmission electron microscopy with atomic resolution under atmospheric pressures. *MRS Commun.* **7,** 798–812 (2017).

89. Yeadon, M., Yang, J. C., Averback, R. S., Bullard, J. W., Olynick, D. L. & Gibson, J. M. In-situ observations of classical grain growth mechanisms during sintering of copper nanoparticles on (001) copper. *Appl. Phys. Lett* **71,** 4 (1997).

90. Zimmermann, C. G., Yeadon, M., Nordlund, K., Gibson, J. M., Averback, R. S., Herr, U. & Samwer, K. Burrowing of Co Nanoparticles on Clean Cu and Ag Surfaces. *Phys. Rev. Lett.* **83,** 1163–1166 (1999).

91. Tripathi, M., Mittelberger, A., Mustonen, K., Mangler, C., Kotakoski, J., Meyer, J. C. & Susi, T. Cleaning graphene: Comparing heat treatments in air and in vacuum. *Phys. status solidi - Rapid Res. Lett.* **11,** 1700124 (2017).

92. Tanaka, M., Han, M., Takeguchi, M., Chu, F., Shimojo, M., Mitsuishi, K. & Furuya, K. Morphology of iron silicide nanorods formed by electron-beam-induced deposition using ultrahigh-vacuum transmission electron microscope. *Jpn. J. Appl. Phys.* **44,** 5635–5638 (2005).

93. Heim, K. R., Healy, S. D. & Yang, Z. J. Correlations between ultrathin film microstructure and magnetic properties for room temperature epitaxial films of fcc Fe/ Cu(100). *J. Appl. Phys.* **74,** 7422 (1993).

94. Tanishiro, Y., Kanamori, H., Takayanagi, K., Yagi, K. & Honjo, G. UHV Transmission electron microscopy on the reconstructed surface of (111) gold. *Surf. Sci.* **111,** 295–413 (1981).

95. Takayanagi, K. High resolution surface study by in-situ UHV transmission electron microscopy. *Ultramicroscopy* **8,** 145–161 (1982).

96. Takayanagi, K. & Yagi, K. Monatom High Level Electron Microsopy of Metal Surfaces. *Trans. Japan Inst. Met.* **24,** 337–348 (1983).

97. Lu, Q., Wang, A. L., Gong, Y., Hao, W., Cheng, H., Chen, J., Li, B., Yang, N., Niu, W., Wang, J., Yu, Y., Zhang, X., Chen, Y., Fan, Z., Wu, X. J., Chen, J., Luo, J., Li, S., Gu, L. & Zhang, H. Crystal phase-based epitaxial growth of hybrid noble metal nanostructures on 4H/fcc Au nanowires. *Nat. Chem.* **10,** 456–461 (2018).

98. Anton, R. Nucleation and growth of Pd-Au alloy particles on crystalline graphite at elevated temperatures. *Phys. Rev. B* **70,** 245405 (2004).

99. Anton, R. & Kreutzer, P. In situ TEM evaluation of the growth kinetics of Au particles on highly oriented pyrolithic graphite at elevated temperatures. *Phys. Rev. B* **61,** 23 (2000).

100. Yeadon, M., Yang, J. C., Averback, R. S., Bullard, J. W. & Gibson, J. M. Sintering of silver and copper nanoparticles on (001) copper observed by in-situ ultrahigh vacuum transmission electron microscopy. *Nanostructured Mater.* **10,** 731–739 (1998).

101. Yeadon, M., Yang, J. C., Averback, R. S., Bullard, J. W., Olynick, D. L. & Gibson, J. M. In-situ observations of classical grain growth mechanisms during sintering of copper nanoparticles on (001) copper. *Appl. Phys. Lett.* **71,** 1631–1633 (1997).

102. Reidy, K., Thomsen, J. D., Lee, H. Y., Zarubin, V., Yu, Y., Wang, B., Pham, T., Periwal, P. & Ross, F. M. Mechanisms of Quasi van der Waals Epitaxy of Three-Dimensional Metallic Nanoislands on Suspended Two-Dimensional Materials. *Nano Lett.* **22,** 5849–5858 (2022).

103. Zagler, G., Trentino, A., Mustonen, K., Mangler, C. & Kotakoski, J. Interface effects on titanium growth on graphene. *ArXiv* (2022). doi:arxiv.org/abs/2204.09669

104. Thomsen, J. D., Reidy, K., Pham, T., Klein, J., Osherov, A., Dana, R. & Ross, F. M. Suspended Graphene Membranes to Control Au Nucleation and Growth. *ACS Nano* **16,** 10364–10371 (2022).

105. Reidy, K., Varnavides, G., Dahl Thomsen, J., Kumar, A., Pham, T., Blackburn, A. M., Anikeeva, P., Narang, P., Lebeau, J. M. & Ross, F. M. Direct imaging and electronic structure modulation of moiré superlattices at the 2D/3D interface. *Nat. Commun.* **12,** 1290 (2021).

106. Ross, F. M., Tersoff, J. & Reuter, M. C. Sawtooth faceting in silicon nanowires. *Phys. Rev. Lett.* **95,** 146104 (2005).

107. Wen, C.-Y., Reuter, M. C., Bruley, J., Tersoff, J., Kodambaka, S., Stach, E. A. & Ross, F. M. Formation of Compositionally Abrupt Axial Heterojunctions in Silicon-Germanium Nanowires. *Science.* **326,** 1247–1250 (2009).

108. Jacobsson, D., Panciera, F., Tersoff, J., Reuter, M. C., Lehmann, S., Hofmann, S., Dick, K. A. & Ross, F. M. Interface dynamics and crystal phase switching in GaAs nanowires. *Nature* **531,** 317–322 (2016).

109. Yang, P. The Chemistry and Physics of Semiconductor Nanowires. *MRS Bull.* **30,** 85–91 (2005).

110. Periwal, P., Thomsen, J. D., Reidy, K., Varnavides, G., Zakharov, D. N., Gignac, L., Reuter, M. C., Booth, T. J., Hofmann, S. & Ross, F. M. Catalytically mediated epitaxy of 3D semiconductors on van der Waals substrates. *Appl. Phys. Rev.* **7,** 31402 (2020).

111. Eaglesham, D. J. & Cerullo, M. Dislocation-Free Stranski-Krastanow Growth of Ge on Si(100). *Phys. Rev. Lett.* **64,** 16 (1990).

112. Kammler, M., Hull, R., Reuter, M. C. & Ross, F. M. Lateral control of self-assembled island nucleation by focused-ion-beam micropatterning. *Appl. Phys. Lett.* **82,** 1093–1095 (2003).

113. Stach, E. A., Hull, R., Tromp, R. M., Reuter, M. C., Copel, M., LeGoues, F. K. & Bean, J. C. Effect of the surface upon misfit dislocation velocities during the growth and annealing of SiGe/Si (001) heterostructures. *J. Appl. Phys.* **83,** 1931 (1998).

114. Tromp, R. M. & Ross, F. M. Advances in in situ ultra-high vacuum electron microscopy: growth of

SiGe on Si. *Annu. Rev. Mater. Sci* **30,** 431–480 (2000).

115. Ross, F. M. Growth processes and phase transformations studied by in situ transmission electron microscopy. *IBM J. Res. Dev.* **44,** 489–499 (2000).

116. Oshima, Y., Nakade, H., Shigeki, S., Hirayama, H. & Takayanagi, K. UHV-TEM/TED observation of Ag islands grown on Si(1 1 1)$\sqrt{3} \times \sqrt{3}$-Ag surface. *Surf. Sci.* **493,** 366–372 (2001).

117. Fujiwara, S., Tsuji, M., Fujii, Y., Susuki, Y., Kimura, K. & Mannami, M.-H. Epitaxial Growth of Lead Chalcogenides on Tin Telluride (001). *Bull. Inst. Chem. Res., Kyoto Univ* **69,** (1991).

118. Plass, R. & Marks, L. D. UHV transmission electron microscopy structure determination of the Si(111)-(7x7)R30°Au surface. *Surf. Sci.* **342,** 233–249 (1995).

119. Hollensteiner, S., Spiecker, E. & Jäger, W. Metal-induced nanostructures on surfaces of layered chalcogenides. *Appl. Surf. Sci.* **241,** 49–55 (2005).

120. Kavanagh, K., Reuter, M. C. & Tromp, R. M. High-temperature epitaxy of PtSi/Si(0 0 1). *J. Cryst. Growth* **173,** 393–401 (1997).

121. Marks, L. D. & Smith, D. J. Direct surface imaging in small metal particles. *Nature* **303,** 316–317 (1983).

122. Binnig, G., Rohrer, H., Gerber, C. & Weibel, E. 7 × 7 Reconstruction on Si(111) Resolved in Real Space. *Phys. Rev. Lett.* **50,** 120 (1983).

123. Takayanagi, K., Tanishiro, Y., Takahashi, S. & Takahashi, M. Structure analysis of Si(111)-7 × 7 reconstructed surface by transmission electron diffraction. *Surf. Sci.* **164,** 367–392 (1985).

124. Takayanagi, K., Tanishiro, Y. & Takahashi, M. Structural analysis of Si(111)-7×7 by UHV-transmission electron diffraction and microscopy. *J. Vac. Sci. Technol. A* **3,** 1502 (1985).

125. Hamers, R. J., Tromp, R. M. & Demuth, J. E. Surface Electronic Structure of Si (111)-(7×7) Resolved in Real Space. *Phys. Rev. Lett.* **56,** 1972 (1986).

126. Somorjai, G. A. in *Fifty Years Electron Diffr.* (ed. Goodman, P.) 201 (Reidel, Oordrecht, 1982).

127. Zhou, G. W., Wang, L., Birtcher, R. C., Baldo, P. M., Pearson, J. E., Yang, J. C. & Eastman, J. A. Cu_2O Island Shape Transition during Cu-Au Alloy Oxidation. *Phys. Rev. Lett.* **96,** 226108 (2006).

128. Li, M., Curnan, M. T., Gresh-Sill, M. A., House, S. D., Saidi, W. A. & Yang, J. C. Unusual layer-by-layer growth of epitaxial oxide islands during Cu oxidation. *Nat. Commun.* **12,** 1–7 (2021).

129. Ross, F. M. & Gibson, J. M. Dynamic Observations of Interface Propagation during Silicon Oxidation. *Phys. Rev. Lett* **68,** 1782–1786 (1992).

130. Ross, F. M., Gibson, J. M. & Twesten, R. D. Dynamic observations of interface motion during the oxidation of silicon. *Surf. Sci.* **310,** 243–266 (1994).

131. Hansen, P. L., Wagner, J. B., Helveg, S., Rostrup-Nielsen, J. R., Clausen, B. S. & Topsøe, H. Atom-Resolved Imaging of Dynamic Shape Changes in Supported Copper Nanocrystals. *Science.* **295,** 2053–2055 (2002).

132. Lv, H., Lin, L., Zhang, X., Song, Y., Matsumoto, H., Zeng, C., Ta, N., Liu, W., Gao, D., Wang, G. & Bao, X. In Situ Investigation of Reversible Exsolution/Dissolution of CoFe Alloy Nanoparticles in a Co-Doped $Sr_2Fe_{1.5}Mo_{0.5}O_{6-\delta}$ Cathode for CO_2 Electrolysis. *Adv. Mater.* **32,** (2020).

133. Jiang, Q., Luo, W., Piao, Y., Matsumoto, H., Liu, X., Zü, A., Parkhomenko, K., Pham-Huu, C. & Liu, Y. Surface Oxygenate Species on TiC Reinforce Cobalt-Catalyzed Fischer−Tropsch Synthesis. *ACS Catal.* **22,** 25 (2022).

134. Zhang, X., Han, S., Zhu, B., Zhang, G., Li, X., Gao, Y., Wu, Z., Yang, B., Liu, Y., Baaziz, W., Ersen, O., Gu, M., Miller, J. T. & Liu, W. Reversible loss of core–shell structure for Ni–Au bimetallic

nanoparticles during CO_2 hydrogenation. *Nat. Catal.* **3,** 411–417 (2020).

135. Hobbs, L. W. Electron-beam sensitivity in inorganic specimens. *Ultramicroscopy* **23,** 339–344 (1987).

136. Egerton, R. F., Li, P. & Malac, M. Radiation damage in the TEM and SEM. *Micron* **35,** 399–409 (2004).

137. Joy, D. C. Future of e-beam metrology: obstacles and opportunities. *Metrol. Insp. Process Control Microlithogr.* **4689,** 1–10 (2002).

138. Joy, D. C. *Monte Carlo Modeling for Electron Microscopy and Microanalysis*. (Oxford University Press, 1995).

139. Jones, L., Yang, H., Pennycook, T. J., Marshall, M. S. J., Van Aert, S., Browning, N. D., Castell, M. R. & Nellist, P. D. Smart Align—a new tool for robust non-rigid registration of scanning microscope data. *Adv. Struct. Chem. Imaging* **1,** 8 (2015).

140. Stevens, A., Yang, H., Carin, L., Arslan, I. & Browning, N. D. The potential for Bayesian compressive sensing to significantly reduce electron dose in high-resolution STEM images. *Microscopy* **63,** 41–51 (2014).

141. Howie, A. Progress Towards More Realistic In-Situ Microscopy Observations. *Micros. Today* **1,** 5–7 (2002).

142. De Jonge, N., Bigelow, W. C. & Veith, G. M. Atmospheric Pressure Scanning Transmission Electron Microscopy. *Nano Lett.* **10,** 1028–1031 (2010).

143. Danilatos, G. D. Optimum beam transfer in the environmental scanning electron microscope. *J. Microsc.* **234,** 26–37 (2009).

144. Hofmann, S., Sharma, R., Ducati, C., Du, G., Mattevi, C., Cepek, C., Cantoro, M., Pisana, S., Parvez, A., Cervantes-Sodi, F., Ferrari, A. C., Dunin-Borkowski, R., Lizzit, S., Petaccia, L., Goldoni, A. & Robertson, J. In situ observations of catalyst dynamics during surface-bound carbon nanotube nucleation. *Nano Lett.* **7,** 602–608 (2007).

145. Mills, M. J., Baluc, N. L. & Sarosi, P. M. HRTEM of dislocation cores and thin-foil effects in metals and intermetallic compounds. *Microsc. Res. Tech.* **69,** 317–329 (2006).

146. Bricknell, R. H. & Melton, K. N. Thin foil electron microscope observations on NiTiCu shape memory alloys. *Metall. Trans. A 1980 119* **11,** 1541–1546 (1980).

147. Rao, L. L. R., Singha, M. K., Subramaniam, K. M., Jampana, N. & Asokan, S. Molybdenum Microheaters for MEMS-Based Gas Sensor Applications: Fabrication, Electro-Thermo-Mechanical and Response Characterization. *IEEE Sens. J.* **17,** 22–29 (2017).

148. Creemer, J. F., Briand, D., Zandbergen, H. W., van der Vlist, W., de Boer, C. R., de Rooij, N. F. & Sarro, P. M. Microhotplates with TiN heaters. *Sensors Actuators A Phys.* **148,** 416–421 (2008).

149. Mecklenburg, M., Hubbard, W. A., White, E. R., Dhall, R., Cronin, S. B., Aloni, S. & Regan, B. C. Nanoscale temperature mapping in operating microelectronic devices. *Science.* **347,** 629–632 (2015).

150. Idrobo, J. C., Lupini, A. R., Feng, T., Unocic, R. R., Walden, F. S., Gardiner, D. S., Lovejoy, T. C., Dellby, N., Pantelides, S. T. & Krivanek, O. L. Temperature Measurement by a Nanoscale Electron Probe Using Energy Gain and Loss Spectroscopy. *Phys. Rev. Lett.* **120,** 095901 (2018).

151. Tornberg, M., Maliakkal, C. B., Jacobsson, D., Wallenberg, R. & Dick, K. A. Enabling In Situ Studies of Metal-Organic Chemical Vapor Deposition in a Transmission Electron Microscope. *Microsc. Microanal.* **28,** 1484–1492 (2022).

152. Wehmeyer, G., Bustillo, K. C., Minor, A. M. & Dames, C. Measuring temperature-dependent thermal diffuse scattering using scanning transmission electron microscopy. *Appl. Phys. Lett.* **113,** 253101 (2018).

153. Wu, F. & Yao, N. Advances in windowed gas cells for in-situ TEM studies. *Nano Energy* **13,** 735–756 (2015).

154. Mehraeen, S., McKeown, J. T., Deshmukh, P. V., Evans, J. E., Abellan, P., Xu, P., Reed, B. W., Taheri, M. L., Fischione, P. E. & Browning, N. D. A (S)TEM Gas Cell Holder with Localized Laser Heating for In Situ Experiments. *Microsc. Microanal.* **19,** 470–478 (2013).

155. Zhang, Y., Howver, R., Gogoi, B. & Yazdi, N. A high-sensitive ultra-thin MEMS capacitive pressure sensor. *2011 16th Int. Solid-State Sensors, Actuators Microsystems Conf. TRANSDUCERS'11* 112–115 (2011). doi:10.1109/TRANSDUCERS.2011.5969151

156. Marsi, N., Majlis, B. Y., Hamzah, A. A. & Mohd-Yasin, F. Development of high temperature resistant of 500 °C employing silicon carbide (3C-SiC) based MEMS pressure sensor. *Microsyst. Technol. 2014 212* **21,** 319–330 (2014).

157. Hermann, G., Coudray, N., Buessler, J. L., Caujolle-Bert, D., Rémigy, H. W. & Urban, J. P. ANIMATED-TEM: A toolbox for electron microscope automation based on image analysis. *Mach. Vis. Appl.* **23,** 691–711 (2012).

158. Xu, M., Kumar, A. & Lebeau, J. Automating Electron Microscopy through Machine Learning and USETEM. *Microsc. Microanal* **27,** 2021 (2022).

159. Rosi, P., Clausen, A., Weber, D., Tavabi, A. H., Frabboni, S., Tiemeijer, P., Dunin-Borkowski, R. E., Rotunno, E. & Grillo, V. Automatic alignment of an orbital angular momentum sorter in a transmission electron microscope using a convolution neural network. (2021). at <https://arxiv.org/abs/2111.05032v1>

160. Mukherjee, D., Roccapriore, K. M., Al-Najjar, A., Ghosh, A., Hinkle, J. D., Lupini, A. R., Vasudevan, R. K., Kalinin, S. V., Ovchinnikova, O. S., Ziatdinov, M. A. & Rao, N. S. A Roadmap for Edge Computing Enabled Automated Multidimensional Transmission Electron Microscopy. *Micros. Today* **30,** 10–19 (2022).

161. Oostergetel, G. T., Keegstra, W. & Brisson, A. Automation of specimen selection and data acquisition for protein electron crystallography. *Ultramicroscopy* **74,** 47–59 (1998).

162. Carragher, B., Fellmann, D., Kisseberth, N., Milligan, R. A., Potter, C. S., Pulokas, J. & Zhu, Y. Automation for Cryo-TEM: from Specimen Grid to 3D Map. *Microsc. Microanal.* **7,** 970–971 (2001).

163. Strauss, M., Arjavac, J., Horspool, D., Nakahara, K., Deeb, C., Strauss, al M., Horspool, D. N. & Hobbs, C. Automated S/TEM metrology on advanced semiconductor gate structures. *Proc. SPIE 8324, Metrol. Insp. Process Control Microlithogr.* **8324,** 346–357 (2012).

164. Spurgeon, S. R., Ophus, C., Jones, L., Petford-Long, A., Kalinin, S. V., Olszta, M. J., Dunin-Borkowski, R. E., Salmon, N., Hattar, K., Yang, W. C. D., Sharma, R., Du, Y., Chiaramonti, A., Zheng, H., Buck, E. C., Kovarik, L., Penn, R. L., Li, D., Zhang, X., Murayama, M. & Taheri, M. L. Towards data-driven next-generation transmission electron microscopy. *Nat. Mater.* **20,** 274–279 (2020).

165. Ziatdinov, M., Dyck, O., Maksov, A., Li, X., Sang, X., Xiao, K., Unocic, R. R., Vasudevan, R., Jesse, S. & Kalinin, S. V. Deep Learning of Atomically Resolved Scanning Transmission Electron Microscopy Images: Chemical Identification and Tracking Local Transformations. *ACS Nano* **11,** 12742–12752 (2017).

166. Lee, C. H., Khan, A., Luo, D., Santos, T. P., Shi, C., Janicek, B. E., Kang, S., Zhu, W., Sobh, N. A., Schleife, A., Clark, B. K. & Huang, P. Y. Deep learning enabled strain mapping of single-atom defects in two-dimensional transition metal dichalcogenides with sub-picometer precision. *Nano Lett.* **20,** 3369–3377 (2020).

167. Booth, C. R., Mooney, P. E., Lee, B. C., Lent, M. & Gubbens, A. J. K2: A Super-Resolution Electron Counting Direct Detection Camera for Cryo-EM. *Microsc. Microanal.* **18,** 78–79 (2012).

168. Tate, M. W., Purohit, P., Chamberlain, D., Nguyen, K. X., Hovden, R., Chang, C. S., Deb, P., Turgut, E., Heron, J. T., Schlom, D. G., Ralph, D. C., Fuchs, G. D., Shanks, K. S., Philipp, H. T., Muller, D. A.

& Gruner, S. M. High Dynamic Range Pixel Array Detector for Scanning Transmission Electron Microscopy. *Microsc. Microanal.* **22,** 237–249 (2016).

169. Ortega, E., Nicholls, D., Browning, N. D. & de Jonge, N. High temporal-resolution scanning transmission electron microscopy using sparse-serpentine scan pathways. *Sci. Reports 2021 111* **11,** 1–9 (2021).

170. Ophus, C., Ercius, P., Sarahan, M., Czarnik, C. & Ciston, J. Recording and using 4D-STEM datasets in materials science. *Microsc. Microanal.* **20,** 62–63 (2014).

171. Savitzky, B. H., Hughes, L. A., Zeltmann, S. E., Brown, H. G., Zhao, S., Pelz, P. M., Barnard, E. S., Donohue, J., DaCosta, L. R., Pekin, T. C., Kennedy, E., Janish, M. T., Schneider, M. M., Herring, P., Gopal, C., Anapolsky, A., Ercius, P., Scott, M., Ciston, J., Minor, A. M. & Ophus, C. py4DSTEM: a software package for multimodal analysis of four-dimensional scanning transmission electron microscopy datasets. (2020). at <http://arxiv.org/abs/2003.09523>

172. Peña, F. de la, Prestat, E., Fauske, V. T., Burdet, P., Lähnemann, J., Jokubauskas, P., Furnival, T., Nord, M., Ostasevicius, T., MacArthur, K. E., Johnstone, D. N., Sarahan, M., Taillon, J., Aarholt, T., Migunov, V., Eljarrat, A., Caron, J., Francis, C., Nemoto, T., Poon, T., Mazzucco, S., Tappy, N., Cautaerts, N., Somnath, S., Slater, T., Walls, M., Winkler, F. & Ånes, H. W. hyperspy/hyperspy: Release v1.7.3. (2022). doi:10.5281/ZENODO.7263263

173. Home - OpenCV. at <https://opencv.org/>

174. Ziatdinov, M., Dyck, O., Li, X., Sumpter, B. G., Jesse, S., Vasudevan, R. K. & Kalinin, S. V. Building and exploring libraries of atomic defects in graphene: Scanning transmission electron and scanning tunneling microscopy study. *Sci. Adv.* **5,** (2019).

175. Phatak, C., Petford-Long, A. K. & De Graef, M. Recent Advances in Lorentz Microscopy. (2015). at <http://www.elsevier.com/open-access/userlicense/1.0/>

176. Zheng, F., Kovács, A., Denneulin, T., Caron, J., Weßels, T. & Dunin-Borkowski, R. E. Magnetic Field Mapping using Off-Axis Electron Holography in the Transmission Electron Microscope. *JoVE (Journal Vis. Exp.* e61907 (2020). doi:10.3791/61907

177. Gao, S., Wang, P., Zhang, F., Martinez, G. T., Nellist, P. D., Pan, X. & Kirkland, A. I. Electron ptychographic microscopy for three-dimensional imaging. *Nat. Commun.* **8,** (2017).

178. Jiang, Y., Chen, Z., Han, Y., Deb, P., Gao, H., Xie, S., Purohit, P., Tate, M. W., Park, J., Gruner, S. M., Elser, V. & Muller, D. A. Electron ptychography of 2D materials to deep sub-ångström resolution. *Nature* **559,** 343–349 (2018).

179. Shibata, N., Findlay, S. D., Kohno, Y., Sawada, H., Kondo, Y. & Ikuhara, Y. Differential phase-contrast microscopy at atomic resolution. *Nat. Phys.* **8,** 611–615 (2012).

180. Ophus, C. Four-Dimensional Scanning Transmission Electron Microscopy (4D-STEM): From Scanning Nanodiffraction to Ptychography and Beyond. *Microsc. Microanal.* **25,** 563–582 (2019).

181. De Graef, M. Recent Progress in Lorentz Transmission Electron Microscopy. *ESOMAT* **1,** 01002 (2009).

182. Han, M. G., Garlow, J. A., Liu, Y., Zhang, H., Li, J., Dimarzio, D., Knight, M. W., Petrovic, C., Jariwala, D. & Zhu, Y. Topological Magnetic-Spin Textures in Two-Dimensional van der Waals Cr2Ge2Te6. *Nano Lett.* **19,** 7859–7865 (2019).

183. Idrobo, J. C. A new resolution quest in electron microscopy. *Nat. Rev. Mater. 2020 62* **6,** 100–102 (2020).

184. Huang, C., Borisenko, K. B. & Kirkland, A. I. Exit wave reconstruction of radiation-sensitive materials from low-dose data. *J. Phys. Conf. Ser.* **522,** 012052 (2014).

185. Song, J., Allen, C. S., Gao, S., Huang, C., Sawada, H., Pan, X., Warner, J., Wang, P. & Kirkland, A. I.

Atomic Resolution Defocused Electron Ptychography at Low Dose with a Fast, Direct Electron Detector. *Sci. Reports 2019 91* **9,** 1–8 (2019).

186. Chen, Z., Odstrcil, M., Jiang, Y., Han, Y., Chiu, M. H., Li, L. J. & Muller, D. A. Mixed-state electron ptychography enables sub-angstrom resolution imaging with picometer precision at low dose. *Nat. Commun.* **11,** 1–10 (2020).

187. Krivanek, O. L., Lovejoy, T. C., Dellby, N., Aoki, T., Carpenter, R. W., Rez, P., Soignard, E., Zhu, J., Batson, P. E., Lagos, M. J., Egerton, R. F. & Crozier, P. A. Vibrational spectroscopy in the electron microscope. *Nature* **514,** 209–212 (2014).

188. Urban, K. W., Mayer, J., Jinschek, J. R., Neish, M. J., Lugg, N. R. & Allen, L. J. Achromatic elemental mapping beyond the nanoscale in the transmission electron microscope. *Phys. Rev. Lett.* **110,** 185507 (2013).

189. Pennycook, S. J. & Nellist, P. D. *Scanning transmission electron microscopy*. *Springer Handbooks* (Springer New York, 2019). doi:10.1007/978-3-030-00069-1_2

190. Crozier, P. A. & Chenna, S. In situ analysis of gas composition by electron energy-loss spectroscopy for environmental transmission electron microscopy. *Ultramicroscopy* **111,** 177–185 (2011).

191. Xin, H. L., Pach, E. A., Diaz, R. E., Stach, E. A., Salmeron, M. & Zheng, H. Revealing correlation of valence state with nanoporous structure in cobalt catalyst nanoparticles by in situ environmental TEM. *ACS Nano* **6,** 4241–4247 (2012).

192. Basak, S., Jansen, J., Kabiri, Y. & Zandbergen, H. W. Towards optimization of experimental parameters for studying Li-O2 battery discharge products in TEM using in situ EELS. *Ultramicroscopy* **188,** 52–58 (2018).

193. Persson, A. R., Tornberg, M., Sjökvist, R. & Jacobsson, D. Time-resolved compositional mapping during in situ TEM studies. *Ultramicroscopy* **222,** 113193 (2021).

194. Reidy, K., Majchrzak, P. E., Haas, B., Thomsen, J. D., Konečná, A., Park, E., Klein, J., Jones, A. J. H., Volckaert, K., Biswas, D., Watson, M. D., Cacho, C., Narang, P., Koch, C. T., Ulstrup, S., Ross, F. M. & Idrobo, J. C. Direct Visualization of Subnanometer Variations in the Excitonic Spectra of 2D/3D Semiconductor/Metal Heterostructures. *Nano Lett.* **3,** 1068–1076 (2023).

195. Ek, M., Jespersen, S. P. F., Damsgaard, C. D. & Helveg, S. On the role of the gas environment, electron-dose-rate, and sample on the image resolution in transmission electron microscopy. *Adv. Struct. Chem. Imaging* **2,** 1–8 (2016).

196. Song, B., Schneider, G. F., Xu, Q., Pandraud, G., Dekker, C. & Zandbergen, H. Atomic-scale electron-beam sculpting of near-defect-free graphene nanostructures. *Nano Lett.* **11,** 2247–2250 (2011).

197. Leuthner, G. T., Susi, T., Mangler, C., Meyer, J. C. & Kotakoski, J. Chemistry at graphene edges in the electron microscope. *2D Mater.* **8,** 035023 (2021).

198. Thomsen, J. D., Kling, J., MacKenzie, D. M. A., Bøggild, P. & Booth, T. J. Oxidation of suspended graphene: Etch dynamics and stability beyond 1000 °c. *ACS Nano* **13,** 2281–2288 (2019).

199. Chou, Y. C., Panciera, F., Reuter, M. C., Stach, E. A. & Ross, F. M. Nanowire growth kinetics in aberration corrected environmental transmission electron microscopy. *Chem. Commun.* **52,** 5686–5689 (2016).

200. Freedy, K. M., Beechem, T. E., Litwin, P. M., Sales, M. G., Huang, M., Ruoff, R. S. & McDonnell, S. J. Unraveling Chemical Interactions between Titanium and Graphene for Electrical Contact Applications. *ACS Appl. Nano Mater.* **1,** 4828–4835 (2018).

201. Goodge, B. H., Baek, D. J. & Kourkoutis, L. F. Direct Electron Detection for Atomic Resolution in situ EELS. *Microsc. Microanal.* **24,** 1844–1845 (2018).

202. Carlos Idrobo, J., Konečná, A., Reidy, K., Park, E., Gallina, P., Šikola, T., Ross, F., Javier, F. & De

Abajo, G. Exploring electronic coupling of optical and phonon excitations at the nanoscale. *Microsc. Microanal.* **27,** 1202–1203 (2021).

203. Ophus, C. A fast image simulation algorithm for scanning transmission electron microscopy. *Adv. Struct. Chem. Imaging* **3,** 1–11 (2017).

204. Żak, A. M. Light-Induced in Situ Transmission Electron Microscopy-Development, Challenges, and Perspectives. *Nano Lett.* **22,** 9219–9226 (2022).

205. Kadkhodazadeh, S., Cavalca, F. C., Miller, B. J., Zhang, L., Wagner, J. B., Crozier, P. A. & Hansen, T. W. In Situ TEM under Optical Excitation for Catalysis Research. *Top. Curr. Chem.* **380,** 1–38 (2022).

206. Minor, A. M., Denes, P. & Muller, D. A. Cryogenic electron microscopy for quantum science. *MRS Bull.* **44,** 961–966 (2019).

207. Goodge, B. H., Goodge, B. H., Bianco, E., Schnitzer, N., Zandbergen, H. W., Zandbergen, H. W., Kourkoutis, L. F. & Kourkoutis, L. F. Atomic-Resolution Cryo-STEM Across Continuously Variable Temperatures. *Microsc. Microanal.* **26,** 439–446 (2020).

208. Kaiser, U., Biskupek, J., Meyer, J. C., Leschner, J., Lechner, L., Rose, H., Stöger-Pollach, M., Khlobystov, A. N., Hartel, P., Müller, H., Haider, M., Eyhusen, S. & Benner, G. Transmission electron microscopy at 20 kV for imaging and spectroscopy. *Ultramicroscopy* **111,** 1239–1246 (2011).

209. Morishita, S., Mukai, M., Suenaga, K. & Sawada, H. Atomic Resolution Imaging at an Ultralow Accelerating Voltage by a Monochromatic Transmission Electron Microscope. *Phys. Rev. Lett.* **117,** 153004 (2016).

210. Urban, K. W., Barthel, J., Houben, L., Jia, C.-L., Jin, L., Lentzen, M., Mi, S.-B., Thust, A. & Tillmann, K. Progress in atomic-resolution aberration corrected conventional transmission electron microscopy (CTEM). *Prog. Mater. Sci.* **133,** 101037 (2023).

211. Haider, M., Hartel, P., Müller, H., Uhlemann, S. & Zach, J. Information Transfer in a TEM Corrected for Spherical and Chromatic Aberration. *Microsc. Microanal.* **16,** 393–408 (2010).

212. Miller, D., Dahmen, U. & Stach, E. New opportunities for In situ Science Based on the TEAM Platform . *Microsc. Microanal.* **17,** 450–451 (2011).

213. Borrnert, F., Muller, H., Linck, M., Horst, A., Kirkland, A. I., Buchner, B. & Lichte, H. Approaching the Lab in the Gap: First Results from a Versatile In-situ (S)TEM. *Microsc. Microanal.* **21,** 99–100 (2015).

214. Tian, X., Kim, D. S., Yang, S., Ciccarino, C. J., Gong, Y., Yang, Y., Yang, Y., Duschatko, B., Yuan, Y., Ajayan, P. M., Idrobo, J.-C., Narang, P. & Miao, J. Determining the 3D Atomic Coordinates and Crystal Defects in 2D Materials with Picometer Precision. *Microsc. Microanal.* **25,** 404–405 (2019).

215. Picher, M., Mazzucco, S., Blankenship, S. & Sharma, R. Vibrational and optical spectroscopies integrated with environmental transmission electron microscopy. *Ultramicroscopy* **150,** 10–15 (2015).

216. Lobastov, V. A., Srinivasan, R. & Zewail, A. H. Four-dimensional ultrafast electron microscopy. *Biophys. Chem.* **17,** 7069–7073 (2005).

217. King, W. E., Campbell, G. H., Frank, A., Reed, B., Schmerge, J. F., Siwick, B. J., Stuart, B. C. & Weber, P. M. Ultrafast electron microscopy in materials science, biology, and chemistry. *J. Appl. Phys.* **97,** 111101 (2005).

218. Browning, N. D., Campbell, G. H., Evans, J. E., LaGrange, T. B. & Reed, B. W. Electron Microscopy and Spectroscopy on the Ultrafast Timescale. *ChemPhysChem* **11,** 781–782 (2010).

219. Fu, X., Wang, E., Zhao, Y., Liu, A., Montgomery, E., Gokhale, V. J., Gorman, J. J., Jing, C., Lau, J. W. & Zhu, Y. Direct visualization of electromagnetic wave dynamics by laser-free ultrafast electron microscopy. *Sci. Adv.* **6,** (2020).

220. Doömer, H. & Bostanjoglo, O. High-speed transmission electron microscope. *Rev. Sci. Instrum.* **74,**

4369–4372 (2003).

221. Berger, J. A., Hogan, J. T., Greco, M. J., Schroeder, W. A., Nicholls, A. W. & Browning, N. D. DC Photoelectron Gun Parameters for Ultrafast Electron Microscopy. *Microsc. Microanal.* **15,** 298–313 (2009).

222. Rubiano Da Silva, N., Möller, M., Feist, A., Ulrichs, H., Ropers, C. & Schäfer, S. Nanoscale Mapping of Ultrafast Magnetization Dynamics with Femtosecond Lorentz Microscopy. *Phys. Rev. X* **8,** 031052 (2018).

223. Möller, M., Gaida, J. H., Schäfer, S. & Ropers, C. Few-nm tracking of current-driven magnetic vortex orbits using ultrafast Lorentz microscopy. *Commun. Phys. 2020 31* **3,** 1–7 (2020).

224. Ohnishi, H., Kondo, Y. & Takayanagi, K. Quantized conductance through individual rows of suspended gold atoms. *Nature* **395,** 780–783 (1998).

225. Belkacem, A., Friend, C., Zhu, Y., Bare, S. R., Glotzer, S., Petford-Long, A., Ross, F. M., Schlögl, R., Sethian, J., Stach, E. A., Crozier, P., Jenks, C., Nuzzo, R., Ogilvie, J., Fenter, P., Hess, W., Neaton, J., de la Cruz, M. O., Settersten, T., Garrett, B., Horton, L., Kerch, H., Krause, J., Lee, P., Maracas, G., McLean, G., Miranda, R., Haines, J., Runkles, K., Summers, M., Hadley, C. & Edgar, J. Basic Research Needs for Innovation and Discovery of Transformative Experimental Tools. (2016). doi:10.2172/1616508

226. Chen, Z., Turgut, E., Jiang, Y., Nguyen, K. X., Stolt, M. J., Jin, S., Ralph, D. C., Fuchs, G. D. & Muller, D. A. Lorentz electron ptychography for imaging magnetic textures beyond the diffraction limit. *Nat. Nanotechnol. 2022 1711* **17,** 1165–1170 (2022).

227. Mohan, S., Manzorro, R., Vincent, J. L., Tang, B., Sheth, D. Y., Simoncelli, E. P., Matteson, D. S., Crozier, P. A. & Fernandez-Granda, C. Deep Denoising for Scientific Discovery: A Case Study in Electron Microscopy. *IEEE Trans. Comput. Imaging* **8,** 585–597 (2022).

228. Samarth, N. Quantum materials discovery from a synthesis perspective. *Nat. Mater.* **16,** 1068–1076 (2017).

229. Hart, J. L. & Cha, J. J. Seeing Quantum Materials with Cryogenic Transmission Electron Microscopy. *Nano Lett.* **21,** 5449–5452 (2021).

230. Moler, K. A. Imaging quantum materials. *Nat. Mater. 2017 1611* **16,** 1049–1052 (2017).

231. Dagotto, E. Complexity in strongly correlated electronic systems. *Science.* **309,** 257–262 (2005).

232. Bianco, E. & Kourkoutis, L. F. Atomic-Resolution Cryogenic Scanning Transmission Electron Microscopy for Quantum Materials. *Acc. Chem. Res.* **54,** 3277–3287 (2021).

233. Minor, A. M., Denes, P. & Muller, D. A. Cryogenic electron microscopy for quantum science. *MRS Bull.* **44,** 961–966 (2019).

234. Liu, X. & Hersam, M. C. 2D materials for quantum information science. *Nat. Rev. Mater.* **4,** 669–684 (2019).

235. Algara-Siller, G., Kurasch, S., Sedighi, M., Lehtinen, O. & Kaiser, U. The pristine atomic structure of MoS2 monolayer protected from electron radiation damage by graphene. *Appl. Phys. Lett.* **103,** 203107 (2013).

236. Cadiz, F., Courtade, E., Robert, C., Wang, G., Shen, Y., Cai, H., Taniguchi, T., Watanabe, K., Carrere, H., Lagarde, D., Manca, M., Amand, T., Renucci, P., Tongay, S., Marie, X. & Urbaszek, B. Excitonic linewidth approaching the homogeneous limit in MoS_2-Based van der Waals Heterostructures. *Phys. Rev. X* **7,** 1–12 (2017).

237. Shao, F., Woo, S. Y., Wu, N., Schneider, R., Mayne, A. J., De Vasconcellos, S. M., Arora, A., Carey, B. J., Preuß, J. A., Bonnet, N., Och, M., Mattevi, C., Watanabe, K., Taniguchi, T., Niu, Z., Bratschitsch, R. & Tizei, L. H. G. Substrate influence on transition metal dichalcogenide monolayer exciton absorption

linewidth broadening. *Phys. Rev. Mater.* **6,** 074005 (2022).

238. Mccomb, D. W., Lengyel, J. & Carter, C. B. Cryogenic transmission electron microscopy for materials research. *MRS Bull.* **44,** 924–928 (2019).

239. Crozier, P. A., Kourkoutis, L. F., Agar, J., Ercius, P., House, S., Kalinin, S., Mccomb, D., Minor, A., Ogrenci-Memik, S., Ross, F., Scott, M., Scott, T., Taheri, M., Voyles, P., Mccabe, R., Yang, J. & Ying, C. *Enabling Transformative Advances in Energy and Quantum Materials through Development of Novel Approaches to Electron Microscopy*. (2021). at <https://crozier.engineering.asu.edu/wp-content/uploads/2021-NSF-Workshop-Report_Frontiers-in-Electron-Microscopy-3.pdf>

240. Yuan, W., Zhu, B., Li, X. Y., Hansen, T. W., Ou, Y., Fang, K., Yang, H., Zhang, Z., Wagner, J. B., Gao, Y. & Wang, Y. Visualizing H2O molecules reacting at TiO2 active sites with transmission electron microscopy. *Science.* **367,** 428–430 (2020).

241. Yoshida, H., Kuwauchi, Y., Jinschek, J. R., Sun, K., Tanaka, S., Kohyama, M., Shimada, S., Haruta, M. & Takeda, S. Visualizing gas molecules interacting with supported nanoparticulate catalysts at reaction conditions. *Science.* **335,** 317–319 (2012).

242. Hachtel, J. A., Huang, J., Popovs, I., Jansone-Popova, S., Keum, J. K., Jakowski, J., Lovejoy, T. C., Dellby, N., Krivanek, O. L. & Idrobo, J. C. Identification of site-specific isotopic labels by vibrational spectroscopy in the electron microscope. *Science.* **363,** 525–528 (2019).

243. Phillips, P. J., Rui, X., Georgescu, A. B., Disa, A. S., Longo, P., Okunishi, E., Walker, F., Ahn, C. H., Ismail-Beigi, S. & Klie, R. F. Experimental verification of orbital engineering at the atomic scale: Charge transfer and symmetry breaking in nickelate heterostructures. (2017). doi:10.1103/PhysRevB.95.205131

244. Zhao, W., Li, M., Chang, C. Z., Jiang, J., Wu, L., Liu, C., Moodera, J. S., Zhu, Y. & Chan, M. H. W. Direct imaging of electron transfer and its influence on superconducting pairing at FeSe/SrTiO3 interface. *Sci. Adv.* **4,** (2018).

245. Kouchi, A., Furuya, K., Hama, T., Chigai, T., Kozasa, T. & Watanabe, N. Direct Measurements of Activation Energies for Surface Diffusion of CO and CO_2 on Amorphous Solid Water Using In Situ Transmission Electron Microscopy. *Astrophys. J. Lett.* **891,** L22 (2020).

246. Boreyko, J. B., Hansen, R. R., Murphy, K. R., Nath, S., Retterer, S. T. & Collier, C. P. Controlling condensation and frost growth with chemical micropatterns. *Sci. Reports 2016 61* **6,** 1–15 (2016).

247. Schwartz, D. K. Mechanisms and kinetics of self-assembled monolayer formation. *Annu. Rev. Phys. Chem.* **52,** 107–137 (2001).

248. Allers, W., Schwarz, A., Schwarz, U. D. & Wiesendanger, R. Dynamic scanning force microscopy at low temperatures on a noble-gas crystal: Atomic resolution on the xenon(111) surface. *Europhys. Lett.* **48,** 276 (1999).

249. Nowakowska, S., Wäckerlin, A., Kawai, S., Ivas, T., Nowakowski, J., Fatayer, S., Wäckerlin, C., Nijs, T., Meyer, E., Björk, J., Stöhr, M., Gade, L. H. & Jung, T. A. Interplay of weak interactions in the atom-by-atom condensation of xenon within quantum boxes. *Nat. Commun. 2015 61* **6,** 1–6 (2015).